Novel photoresponsive molecules toward photodynamic therapy and protein biosynthesis photocontrol

光応答性分子を用いた光線力学的療法と
蛋白質合成の光制御

March, 2016

AKIYA AKAHOSHI

The Graduate School of
Natural Science and Technology
(Doctor’s Course)

OKAYAMA UNIVERSITY

Contents

Chapter 1

Introduction

Control of biological phenomenon using light such as caged compounds [1], photodynamic therapy (PDT) [2, 3] and photochemical internalization (PCI) [4] have been researched.

Caged compound is protecting group which make bioactive molecules to inactive state, and the temporary inactive molecules recovered by photo-irradiation. Many caged compounds are based on nitrobenzyl group or coumarin group have been reported [5, 6]. These compounds already used at ATP [7], mRNA [8], excitatory transmitter and peptides [9]. However, photoreaction efficacy is not so high, speed of photo-response is slow, and residual products have some toxicity are pointed out. Thus, novel caged compounds improve these matter are expected. Moreover, additional photoresponsive reaction using caged compounds are also desired.

PDT is a minimally invasive technology which is used to treatment for malignant tumor. In the mainly mechanism of PDT, a photosensitizer generates reactive oxygen species (ROS) such as singlet oxygen by photo-irradiation was well known. The singlet oxygen damages to the cell and tissue using light at inherent wavelength. Current photosensitizers are mainly based on porphyrin [10] and chlorophyll [11], and it is essential for modern PDT.

PCI is a technology for release macromolecules from endosome into the cytosol. PCI is also based on use of photosensitizers similar to PDT. This

technology has also been shown to the enhance treatment effect using therapeutic molecules, and epidermal growth factor receptor (EGFR)-targeted therapy has been reported [12]. Application research using PCI was often performed in our laboratory.

In this work, we tried to photocontrol of protein biosynthesis using caged compounds (Chapter 2, Fig. 1-1) and developed DDS carrier for PDT (Chapter 3, Fig. 1-2).

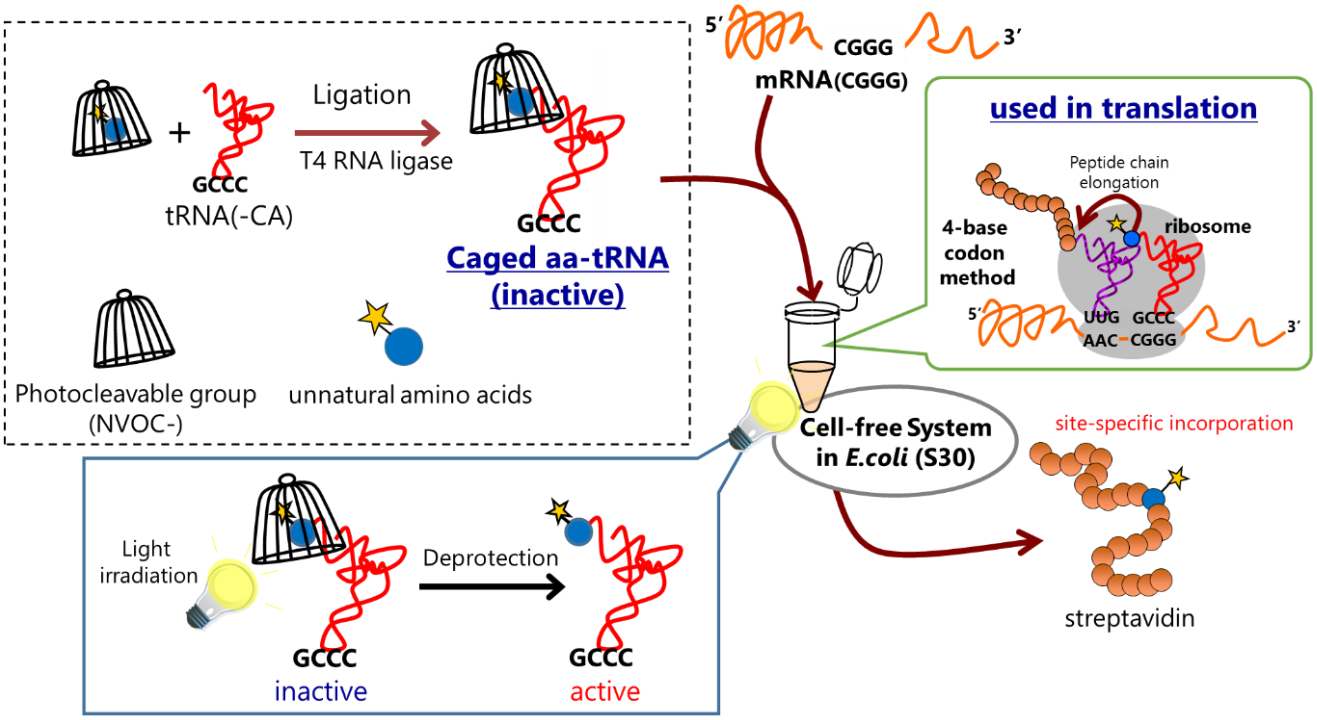

Figure 1-1. Photocontrol of protein biosynthesis (Chapter 2).

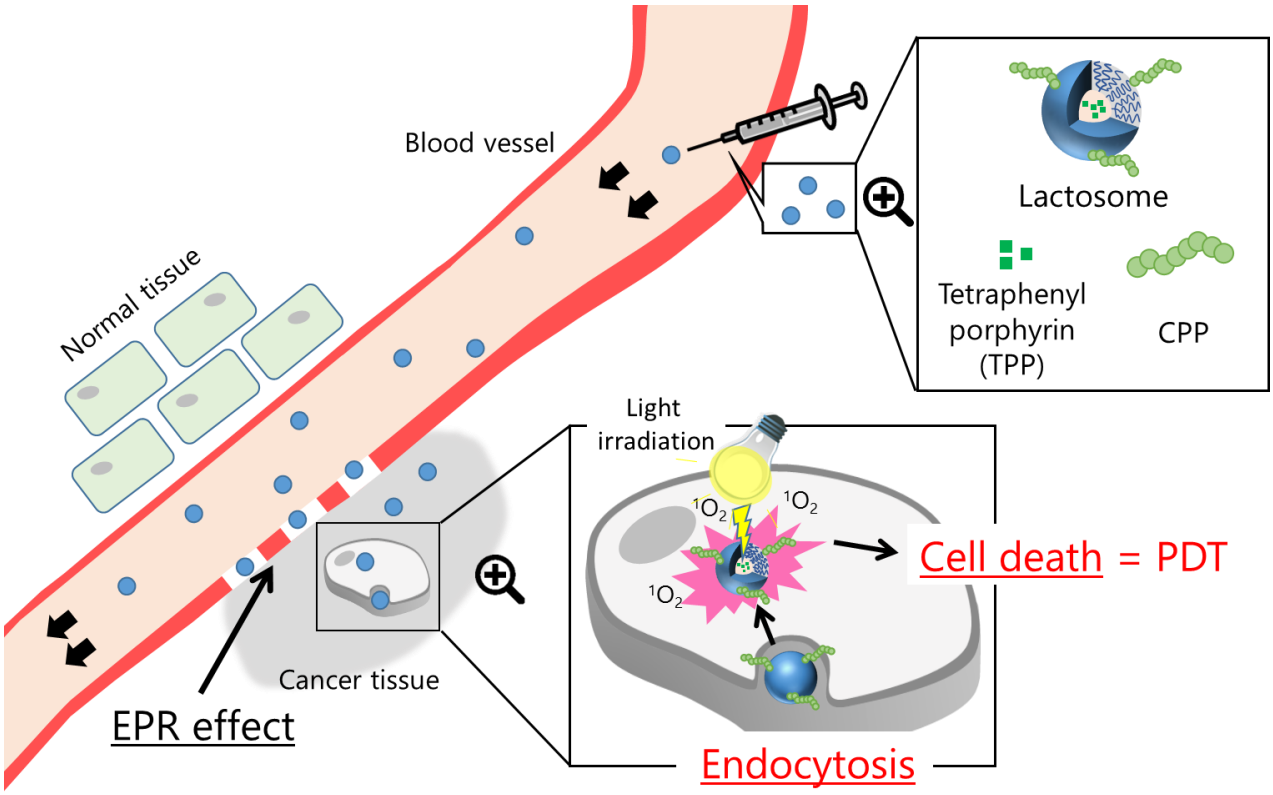

Figure 1-2. Enhanced cellular uptake and PDT in lactosome (Chapter 3).

Detailed backgrounds of "**Protein biosynthesis**", "**Aminoacylation of tRNA using non-natural amino acids**", "**Expanded genetic code**", "**Non-natural amino acids**", "**Caged compounds**" related to Chapter 2 are described in p.5-11. In addition, detailed background of "**Drug delivery system**", "**polymeric micelle**", "**peptides and imaging molecules**", "**photosensitizer**" related to Chapter 3 are described in p.12-15

Protein biosynthesis

DNAs encode RNAs and proteins *in vivo*. An RNA is created using a DNA as a template, and this process is called "transcription". Next, RNA is converted to the protein, and this process is called "translation" (Fig. 1-3 left). A sequence of an amino acid is coded on mRNA. Protein biosynthesis is a process that base arrangement on mRNA is converted to amino acid sequence. A sequence of three nucleotides, called a codon, specifies an amino acid (Fig. 1-3 right). Since there are combinations using 4 possible bases, there are 64 possible codons (4^3 combinations). Sixty-one codons of them correspond to the 20 standard amino acids. AUG orders start of protein biosynthesis, and UAA, UAG and UGA designate the termination of translation. Indeed, various protein is synthesized by the combination of these codons.

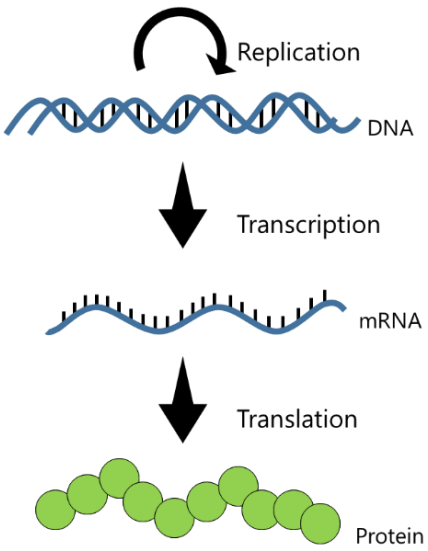

	U		C		A		G	
U	UUU	Phe	UCU	Ser	UAU	Tyr	UGU	Cys
	UUC		UCC		UAC		UGC	
	UUA	Leu	UCA		**UAA**	**Stop**	**UGA**	**Stop**
	UUG		UCG		**UAG**	**Stop**	UGG	Trp
C	CUU	Leu	CCU	Pro	CAU	His	CGU	Arg
	CUC		CCC		CAC		CGC	
	CUA		CCA		CAA	Gln	CGA	
	CUG		CCG		CAG		CGG	
A	AUU	Ile	ACU	Thr	AAU	Asn	AGU	Ser
	AUC		ACC		AAC		AGC	
	AUA		ACA		AAA	Lys	AGA	Arg
	AUG	**Met**	ACG		AAG		AGG	
G	GUU	Val	GCU	Ala	GAU	Asp	GGU	Gly
	GUC		GCC		GAC		GGC	
	GUA		GCA		GAA	Glu	GGA	
	GUG		GCG		GAG		GGG	

Figure 1-3. Central dogma (left) and codon table (right).

Aminoacylation of tRNA using non-natural amino acids

A tRNA is used for incorporation of non-natural amino acids do not have to be aminoacylated by endogenous ARS, while after aminoacylation, aminoacyl-tRNA must efficiently enter into ribosome. The tRNA, inform these orthogonality, have been researched for a long time, and our laboratory discovered orthogonal tRNA for using 4-base codon methods (Fig. 1-4). First step for incorporation of non-natural amino acids is aminoacylation of orthogonal tRNA. We employed the method using pdCpA [13] in this paper. In this pdCpA method, tRNA(-CA) lacking CA sequence from CCA

sequence of 3’-terminas of tRNA and aminoacylated pdCpA dinucleotide are used. Full length aminoacyl-tRNA was obtained from ligation of these two molecules. Advantage of pdCpA is to apply many tRNA and amino acids (or non-natural amino acids). On the other hand, other aminoacylation using misrecognition of ARS can be applied to only some non-natural amino acids whose structure is similar to natural amino acids. Recently, mutant ARS have been developed and improved, however the ARS for amino acids with bulky side chain is stage of research yet.

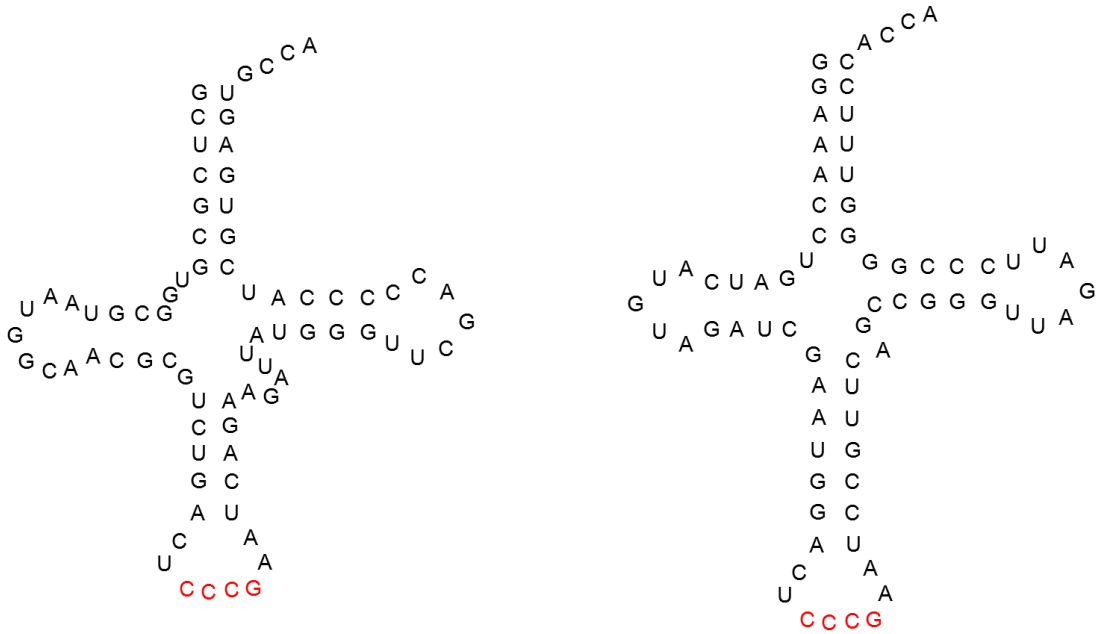

yeast $tRNA^{Arg}_{CCCG}$ Methanosircina acetivorans $tRNA^{Pyl}_{CCCG}$

Figure 1-4. tRNA used by 4-base codon method

Expanded genetic code

For site-specific incorporation of non-natural amino acids, a new codon, which is not normally used as a sense codon, is needed. Amber codon suppression is the most famous method for expanded genetic code [14]. This method use amber codon for incorporation of non-natural amino acids to cell-free translation system and mammalian cells. In 1996, 4-base codon method was reported [15]. Four-base codon method can efficiently incorporate non-natural amino acids to protein using the mRNA with 4-base codon and yeast $tRNA^{Phe}$ which correspond to the mRNA (Fig. 1-5). The 4-base codon has a problem which may be read with 3-base codon, and open reading frame of the codon may slip off by a 1-base. To overcome this problem, Hohsaka et al. designed the mRNA which have a stop codon at downstream of 4-base codon. Advantage of this 4-base codon method against amber codon suppression is to have many usable codons. In fact, 5 types of codons, including CGGG, AGGU and GGGU, show high translation rate in cell-free translation system.

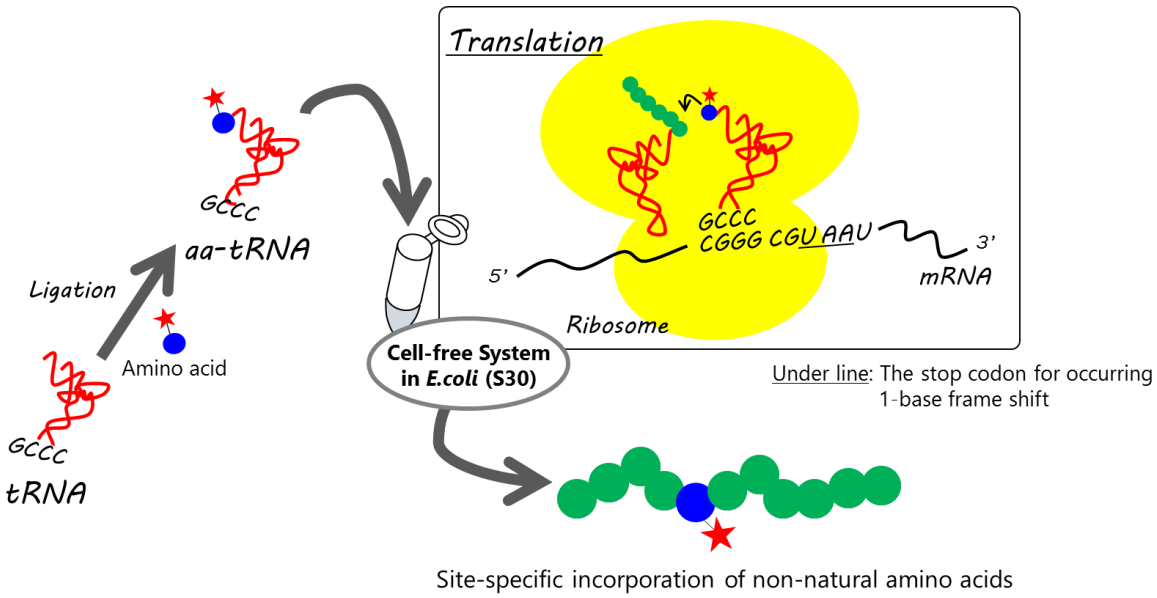

Figure 1-5. Four-base codon method

Non-natural amino acids

Figure 1-6 shows non-natural amino acids which are confirmed to be incorporated into proteins in *E.coli* cell-free translation system. Fluorescent dye modified (BODIPY-labeled) amino acids are also showed in Figure 1-6. Moreover, success of incorporation of other non-natural amino acids which have functional group into protein have been reported.

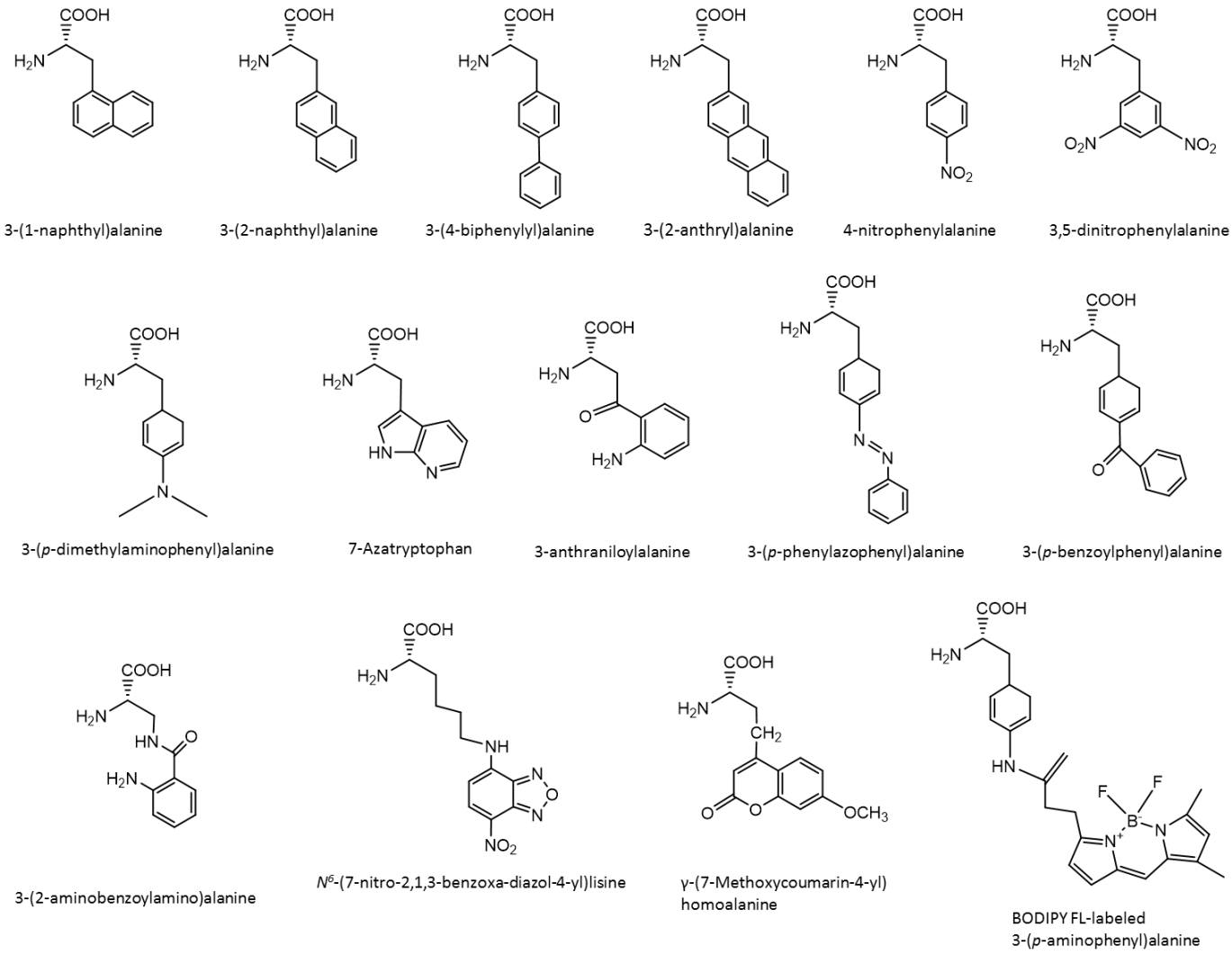

Figure 1-6. Structure of non-natural amino acids examined for incorporation into proteins by using four-base codon method.

Caged compounds

Caged compounds are artificial molecules whose biological activity is controlled by light, and they are synthesized using cage compounds. Cage compounds are protecting groups which make bioactive molecules to inactive state. The temporary inactive molecules with the cage group can become active by photo-irradiation [1]. Caged compounds must have follow three factors.

1) The objective molecules must have functional group which can bind to protect group. There are carboxylic acid, phosphoric acid, sulfonic acid, amide, primary or secondary amine, alcohol, phenol, thiol, ketone, and aldehyde.

2) The biologically active molecules must lose their activity or be inhibited during protection by photocleable group. In 1978, Kaplan et al. reported the first caged compound called NPE-ATP. NPE-ATP was protected γ-phosphoric acid of ATP with 1-(*o*-nitrophenyl)ethyl group (NPE-group) [7]. NPE-ATP could not be used for ATPase-dependent reaction because NPE-group inhibits hydrolysis. After photoirradiation, NPE-group leave from γ-phosphoric acid of ATP, and the ATP can be used for ATPase dependent reaction.

3) Designed caged compounds have to remain stable state in dark place under physiological condition. In the synthesis of caged compounds, many cases of them are often stable state because they are dissolved in an organic solvent.

Thus, the confirmation of stability of caged compounds under physiological condition was essential.

Many photocleable group, *o*-nitrobenzyl group, coumarin-4-ylmethyl group, 2-(*o*-nitrophenyl)-ethyl group and 7-nitroindnitlile group have been reported. These structures were shown in Fig. 1-7. In chapter 2, we selected derivative of *o*-nitrobenzyl group and used them for photocontrol of protein biosynthesis.

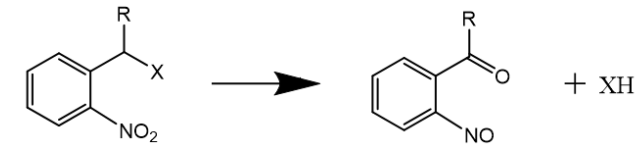

o-nitrobenzyl

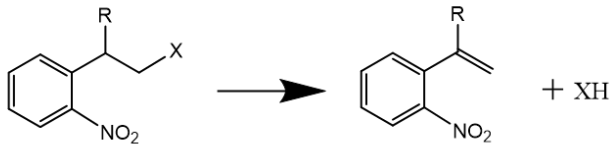

2-(*o*-nitrophenyl)ethyl

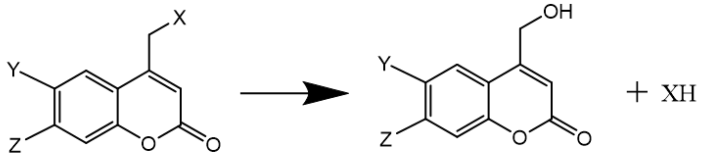

(coumarin-4-yl)methyl

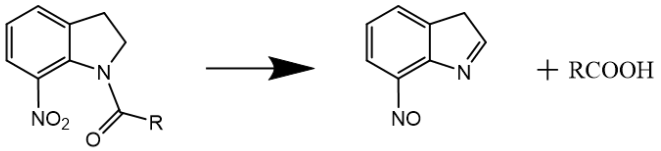

7-nitroindolinyl

Figure 1-7. Structure of photocleavable group

Drug Delivery System (DDS)

DDS is defined as a formulation or a device that enables specific delivery of a therapeutic agent in the body. DDS also improves its efficacy and safety by controlling the rate, time, and place of release. In general, the drug disappears through metabolism by liver or urine excretion after systemic administration. Some drugs can achieve at the objective site, but most of drugs cannot achieve and show the toxicity or the side effect. To overcome this problem, the concept of DDS was proposed in 1960s. Even today, DDS technology is based on this concept, and many researchers study the follow things.

1) Targeting

2) Controlled release

3) Promotion of drug absorption

Over the past few decades, many nanoparticles, including liposomes, polymeric micelles, metal nanoparticles, and dendrimers, have been developed for drug delivery.

Polymeric micelle

In 1970s, Ringsdorf proposed polymeric drug model [16]. Thereafter, several polymeric micelles is based on this model have been developed. Polymeric micelles are composed of hydrophilic polymer and hydrophobic polymer (e.g., polyethylene glycol, polyglycolic acid and polylactic acid), and they can be formed self-assembly in solution for hydrophobic interaction. Polymeric micelles have size of nano-meter and core-shell structure. Furthermore, polymeric micelles can circulate in bloodstream for a long time because they have high solubility and suppress interaction against serum protein. The core of polymeric micelles is able to encapsulate hydrophobic agent because of its high coagulation power. Recently, study for acquisition of several function (e.g., targeting and imaging) of polymer have been performed. In 2009, a new polymeric micelle, called "lactosome", have been developed [17]. Lactosome is composed of polysarcosine and polylactic acid, and both polymer have biodegradability. In fact, we used lactosome in this study (Chapter 3).

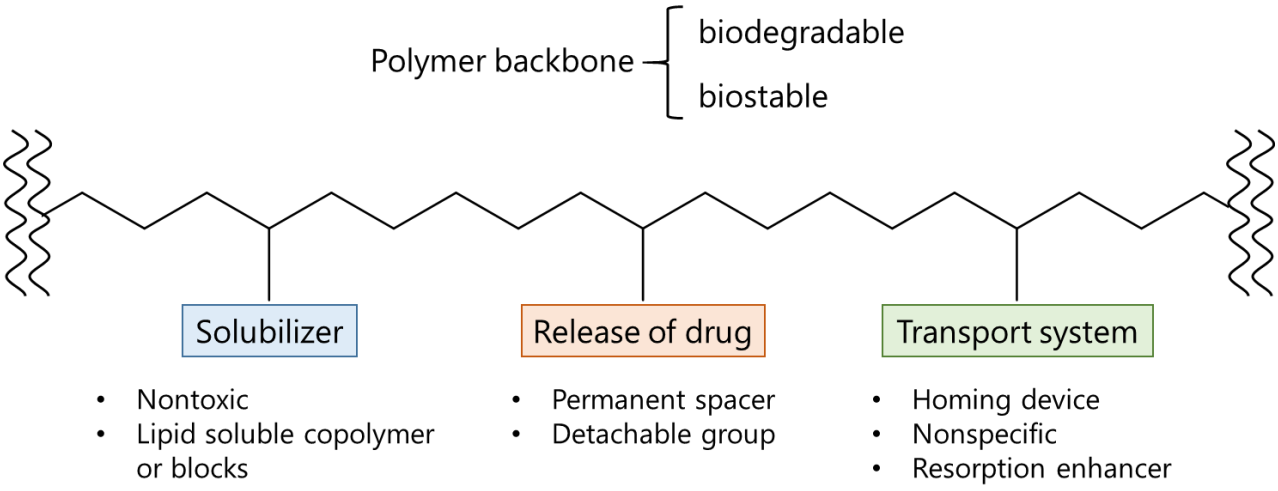

Figure 1-8. Model of polymeric drug by Ringsdorf H.

Peptides and imaging molecules

Cell-penetrating peptide, antibody (for enhanced cellular uptake and targeting), and imaging molecules (e.g., fluorescence molecule and radioactive nuclide) are used for addition of functions to the polymeric micelle described in the previous section. The activity of drug may lower when these molecules directly bond to the drug. However the activity of polymeric micelles does not decrease, because functional molecules can bind to base material of micelles. Thereby, drugs can maintain their activity. Polymeric micelles promise to acquire ability such as targeting, imaging and enhanced cellular uptake.

Photosensitizer

Photosensitizers, such as rose bengal and porphyrin, known to generate reactive oxygen species (ROS) upon excitation by light, have been used for photodynamic therapy (PDT) [18]. PDT is a minimally invasive treatment used for several types of cancers. In the mainly mechanism of PDT, a photosensitizer generates ROS such as singlet oxygen and free radicals by photoirradiation. These ROS damage to the cell and tissue. Most photosensitizers are mainly based on porphyrin and chlorophyll, and it is necessary for modern PDT.

Porphyrin is well known as photosensitizer which induces photoresponsive damage to tumors. There are two mechanisms of action for PDT (*type I* and *type II*). In *type I*, the photosensitizer is excited by light, and the energy state of photosensitizer become higher state. At this point, the excited photosensitizer can act as a reducing agent in the reaction to create ROS. Conversely, the photosensitizer can also act as oxidizing agent by filling the hole vacated by the excited electron. In another mechanism (*type II*), the photosensitizer is also excited with light, but energy is transferred to the triplet ground state of molecular oxygen, and the excited singlet state oxygen has highly cytotoxic [19]. Oxygen is not necessary for *type I*, but oxygen is necessary for *type II*. TPP is derived from porphyrin and has four aryl groups [20]. TPP has no electric charge and shows hydrophobicity, which possesses photosensitizing property similar to porphyrin. In this study, we used TPP and lactosome for drug delivery and PDT. The details are described at Chapter 3.

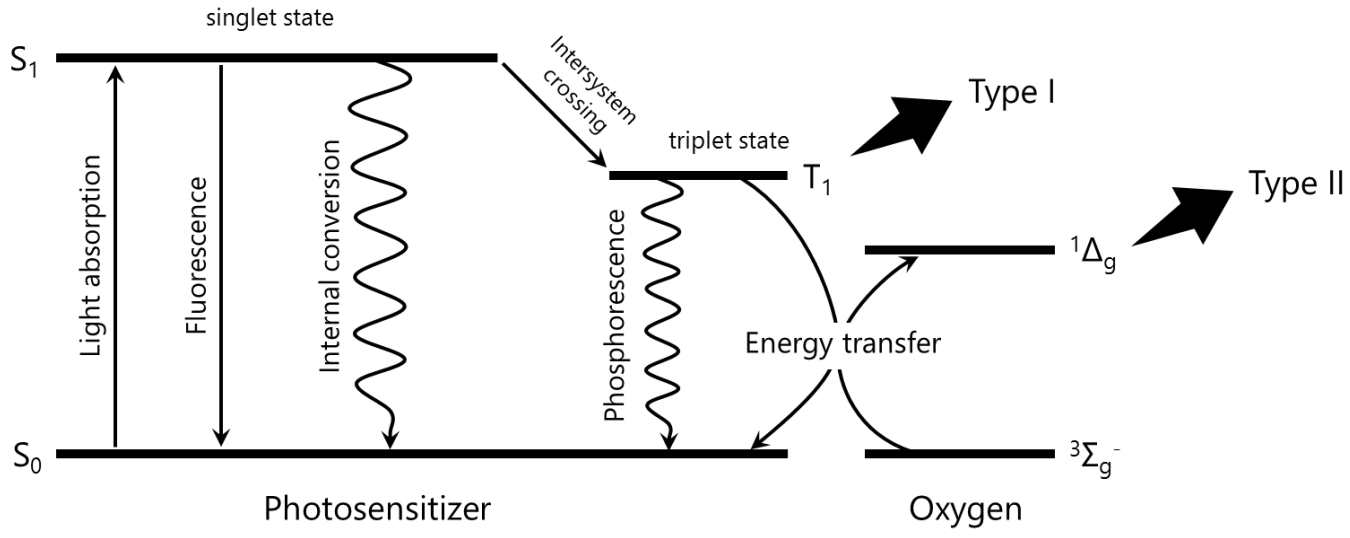

Figure 1-9. A modified Jablonski diagram for PDT

Reference

[1] Ellis-Davies GCR 2007 *Nat. Methods* **4** 619.

[2] Dougherty TJ, Gomer CJ, Henderson BW, Jori G, Kessel D, Korbelik M, Moan J and Peng Q 1998 *J. Natl. Cancer Inst.* **90** 889.

[3] Ethirajan M, Chen Y, Joshi P and Pandey RK 2011 *Chem. Soc. Rev.* **40** 340.

[4] Berg K, Weyergang A, Prasmickaite L, Bonsted A, Hogset A, Strand MT, Wagner E and Selbo PK 2010 *Methods Mol. Biol.* **635** 133.

[5] Aujard I, Benbrahim C, Gouget M, Ruel O, Baudin JB, Neveu P and Jullien L 2006 *Chemistry* **12** 6865.

[6] Robertson SA, Ellman JA and Schultz PG 1991 *J. Am. Chem. Soc.* **113** 2722.

[7] Kaplan JH, Forbush B and Hoffman JF 1978 *Biochemistry* **17** 1929.

[8] Ando H, Furuta T, Tsien RY and Okamoto H 2001 *Nat. Genet.* **28** 317.

[9] Rothman DM, Petersson EJ, Vazquez ME, Brandt GS, Dougherty DA and Imperiali B 2005 *J. Am. Chem. Soc.* **127** 846.

[10] Malik Z and Lugaci H 1987 Br. *J. Cancer* **56** 589.

[11] Henderson BW, Sumlin AB, Owczarczak BL and Dougherty TJ 1991 *J. Photochem. Photobiol.* B, Biol. **10** 303.

[12] Yip WL, Weyergang A, Berg K, Tønnesen HH and Selbo PK 2007 *Mol. Pharm.* **4** 241.

[13] Heckler TG, Chang LH, Zama Y, Naka T, Chorghade MS and Hecht SM 1984 *Biochemistry* **23** 1468.

[14] Noren CJ, Anthony-Cahill SJ, Griffith MC and Schultz PG 1989 *Science* **244** 182.

[15] Hohsaka T, Ashizuka Y, Murakami H and Sisido M 1996 *J. Am. Chem. Soc.* **118** 9778.

[16] Ringsdorf H 1975 *Journal of Polymer Science: Polymer Symposia* **51** 135.

[17] Makino A, Yamahara R, Ozeki E and Kimura S 2007 *Chem. Lett.* **36** 1220.

[18] Gomer CJ 2010 *Methods Mol. Biol.* **635**.

[19] Otsu K, Sato K, Ikeda Y, Imai H, Nakagawa Y, Ohba Y and Fujii J 2005 *Biochem. J.* **389** 197.

[20] Canete M, Villanueva A, Dominguez V, Polo S, Juarranz A and Stockert JC 1998 *Int. J. Oncol.* **13** 497.

Chapter 2

Photo-dependent protein biosynthesis using a caged aminoacyl-tRNA

Introduction

Protein biosynthesis using unique codons, such as four-base codons and the amber codon, has been used for site-specific incorporation of non-natural amino acids into proteins [1-4]. This technology is very useful for functional analysis of proteins and for medicinal chemistry research [5]. For example, incorporation of modified amino acids, such as methylated and phosphorylated amino acids, enabled us to determine how these modifications affected protein function [6]. Site-specific fluorescent labeling of proteins can be used to monitor protein behavior [7], and site-specifically labeled proteins can also be used to screen drug candidates [8].

There is currently a growing interest in developing temporal and/or spatial control of protein synthesis. Photo-regulation of translation has been achieved using caged compounds [9], such as caged mRNA [10] and a photoresponsive 5’-cap [11]. Photo-regulation of translation has also been achieved by siRNA-mediated methods, such as caged siRNA technologies [12-14] and CLIP-RNAi [15-18]. All these methods control the activity or concentration of the target mRNA.

In this study, we prepared caged aminoacyl-tRNAs (aa-tRNAs) bearing a four-base anticodon for photo-dependent translation of an mRNA containing a four-base codon. This is the first report of photo-regulation of translation through the activity of an aa-tRNA. In this caged aa-tRNA, the amino group of amino acid moiety of the aa-tRNA is protected with a

nitroveratryloxycarbonyl (NVOC) group. Since the aminoacyl moiety of the aa-tRNA in the ribosomal A-site reacts with the C-terminus of the growing peptide, the N-protected aa-tRNA cannot be used in the ribosome. Thus, the use of the caged aa-tRNA is expected to enable photo-dependent protein synthesis. Here, we demonstrated that the caged aa-tRNA is stable (i.e., free from deacylation) and could be used for photo-dependent protein synthesis.

Methods and Results

The N-NVOC-aa-tRNA was prepared using NVOC-aminoacyl 5'-phospho 2'-deoxyribocytidiylriboadenosine (pdCpA) and a tRNA lacking the 3'-CA sequence by ligating them with T4 RNA ligase. The NVOC-aminoacyl pdCpA was synthesized using methods similar to Robertson et al [19]. In this study, we used L-2-naphthylalanine (2napAla) as the non-natural amino acid for incorporation into the protein. NVOC-2napAla-pdCpA was prepared, briefly, as follows (Scheme 2-1): First, 2napAla was protected at its α-amino group with the NVOC group. Then, the NVOC-protected 2napAla was reacted with chloroacetonitrile and triethylamine to obtain an NVOC-2napAla cyanomethyl ester. The NVOC-2napAla cyanomethyl ester was reacted with pdCpA to obtain NVOC- 2napAla-pdCpA. NVOC-2napAla-tRNA was prepared by ligating NVOC-2napAla-pdCpA to the *Methanosarcina acetivorans* (MA) $tRNA_{CCCG}$ [20] lacking the 3'-terminal pCpA moiety, as described previously [21]. The preparation of NVOC-caged aa-tRNA for protecting the aa-tRNA from deacylation and for photo-regulation of the protein synthesis is summarized in Scheme 2-2.

To confirm cleavage of the NVOC from the amino acid moiety (2napAla), the fluorescence intensity of NVOC-2napAla-pdCpA was measured before and after UV irradiation (Fig. 2-1A) [22]. Before UV irradiation, the fluorescence of NVOC-2napAla-pdCpA was minimal

because the NVOC group is a quencher [23]. Fluorescence intensity increased after UV irradiation, indicating that the NVOC group was cleaved from NVOC-2napAla-pdCpA, and 2napAla-pdCpA was generated. Figure 2-1A shows the fluorescence of 2napAla-pdCpA over time after UV irradiation. Using this data, concentrations of NVOC-2napAla-pdCpA relative to the initial concentration were calculated for each time point (Fig. 2-1B). The half-life ($t_{1/2}$) of NVOC-2napAla-pdCpA was calculated from Figure 2-1B using the following equations:

$$y = 100\ e^{-kt} \text{ and } t_{1/2} = (\ln 2)/k,$$

where y is the concentration of NVOC-2napAla-pdCpA, k is the rate constant, and t (min) is the irradiation time. The half-life of NVOC-2napAla- pdCpA under UV light was 27.7 min.

Next, the deacylation profiles of the NVOC-aa-tRNA and the aa-tRNA were compared (Fig. 2-2) [24]. In conditions similar to the translation reaction (i.e., 37°C in a neutral buffer), NVOC totally protected the aa-tRNA from deacylation. Although the half-life of 2napAla-tRNA estimated from Figure 2-2 was 114 min, most aa-tRNAs are more unstable [25]. For example, the half-lives of Lys-tRNA and Cys-tRNA are approximately 20 min at 30°C and pH 7.5 [26], and the half-life of Ala-tRNA is 10.9 min at 40°C and pH 7.5 [27]. In particular, aa-tRNAs only deacylate in the absence of a corresponding aminoacyl-tRNA synthetase, which results in inefficient

translation. The aa-tRNAs can be protected against this instability by the addition of the NVOC moiety.

Although the N-protected aa-tRNA cannot be used in the ribosome, it may bind EF-Tu and hinder the use of natural aa-tRNAs by competitive binding to EF-Tu. To examine this possibility, we measured binding of NVOC-2napAla-tRNA to the *Escherichia coli* EF-Tu by a gel-shift analysis [28, 29]. Figure 2-3 shows the gel-shift assay showing EF-Tu binding to the UV-irradiated NVOC-aa-tRNA. EF-Tu did not bind to the NVOC-2napAla-tRNA but did bind to UV-irradiated NVOC-aa-tRNA. This result indicates that UV irradiation induced NVOC cleavage, and the resulting 2napAla-tRNA bound to EF-Tu. Since NVOC-2napAla-tRNA does not bind to EF-Tu, the NVOC derivatized aa-tRNA will not work in a translation system. Thus, the NVOC-aa-tRNA is indeed a caged compound whose bioactivity is totally suppressed in the absence of UV irradiation.

Next, we examined the use of the NVOC-2napAla-$tRNA_{CCCG}$ for protein synthesis in an *in vitro* translation system. A streptavidin (SA) mRNA having a CGGG codon at amino acid position 83 (^{83}CGGG-SA mRNA) was prepared, translated using the NVOC-2napAla-$tRNA_{CCCG}$ and analyzed by Western blotting [30]. The mutated SA mRNA contained an ^{83}CGGG codon and was translated in the presence of NVOC-2napAla-$tRNA_{CCCG}$ when irradiated by UV light (Fig. 2-4A). By contrast, the mutated mRNA was not

translated in the presence of NVOC-2napAla-tRNA$_{CCCG}$ in the absence of UV irradiation. The translation product of the ^{83}CGGG-SA mRNA increased with increasing UV irradiation time (Fig. 2-4B). The synthesis of wild-type SA decreased with increasing UV irradiation, indicating that the translation system was damaged by the UV irradiation. When the translation mixture was irradiated for 45 min, the yield of wild-type SA decreased to approximately 60% relative to the unirradiated translation mixture. Figure 2-4C shows estimates of 2napAla incorporation efficiencies considering the irradiation-time dependent decrease in translation efficiency. The efficiency of 2napAla incorporation after 45 min of UV irradiation was 67%. Photo-dependent protein synthesis using NVOC-caged aa-tRNA was also demonstrated using an enhanced green fluorescent protein (EGFP) mRNA containing a CGGG codon at position 214 (Fig. 2-5) [31]. In this experiment, a natural amino acid (Ser) was introduced into the CGGG codon position of EGFP using NVOC-Ser-tRNA$_{CCCG}$.

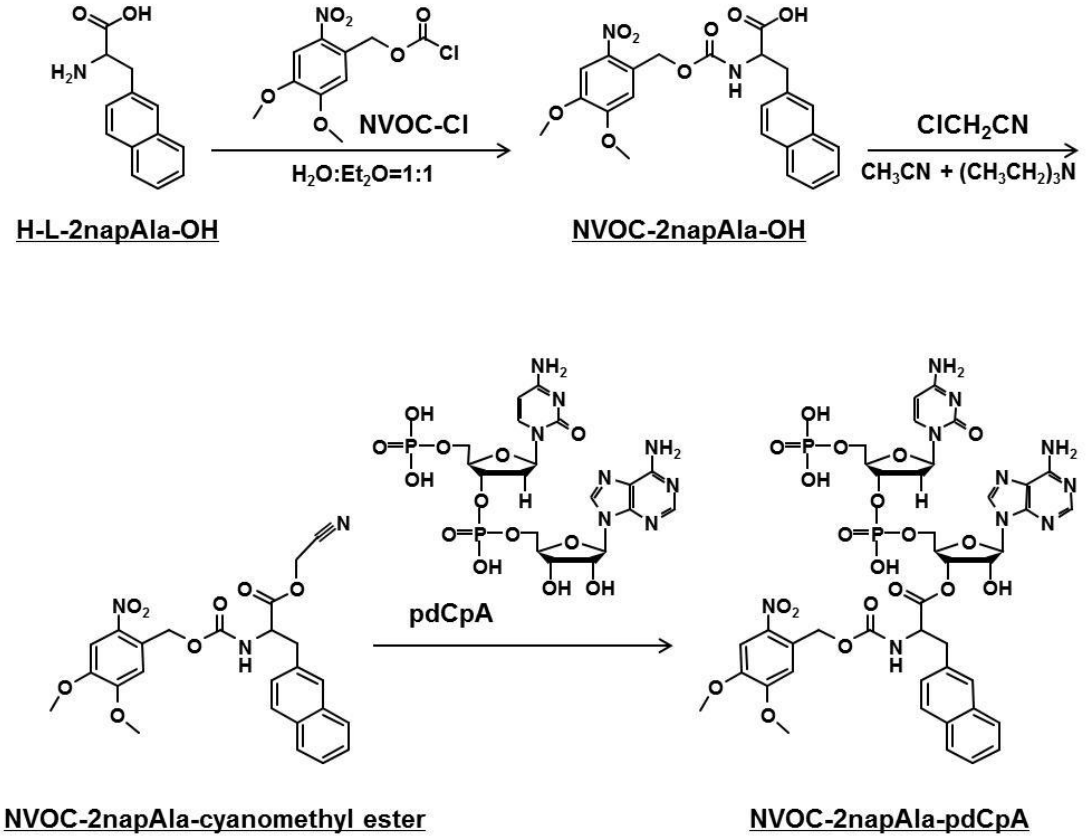

Scheme 2-1. Synthesis of NVOC-2napAla-pdCpA.

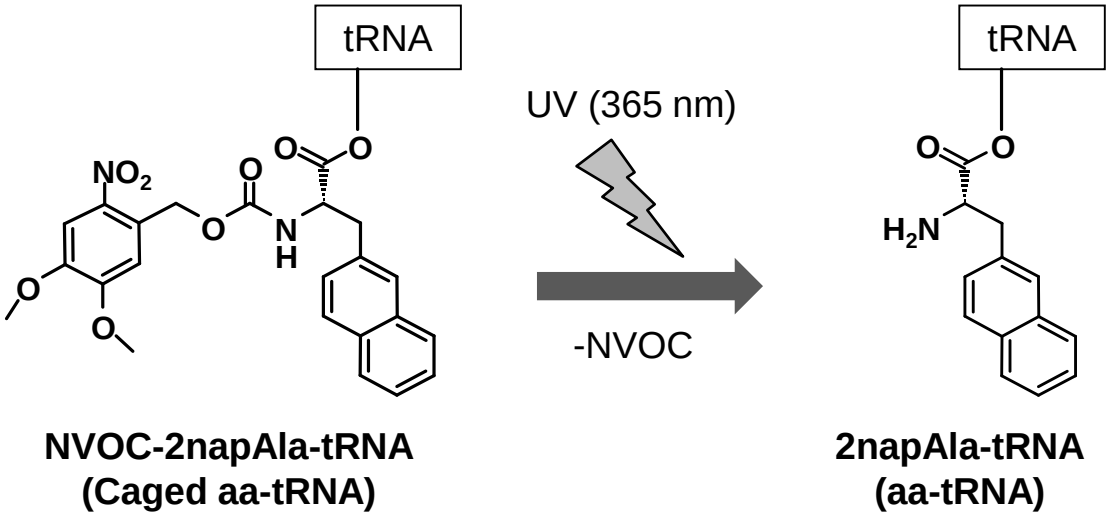

Scheme 2-2. Photo-dependent uncaging of NVOC-2napAla-tRNA.

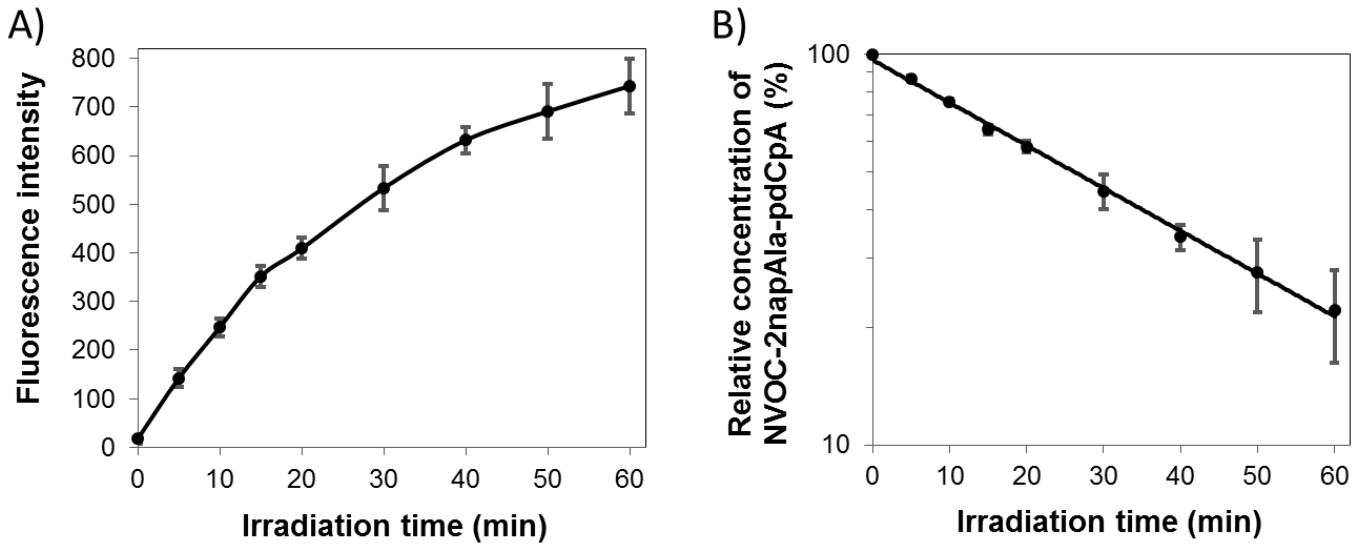

Figure 2-1. NVOC cleavage by UV irradiation.

(A) Fluorescence intensity (λ_{ex} = 270 nm and λ_{em} = 334 nm) of UV-irradiated NVOC-2napAla-pdCpA. (B) Concentration of NVOC-2napAla-pdCpA relative to its concentration at time = 0 min after UV irradiation.

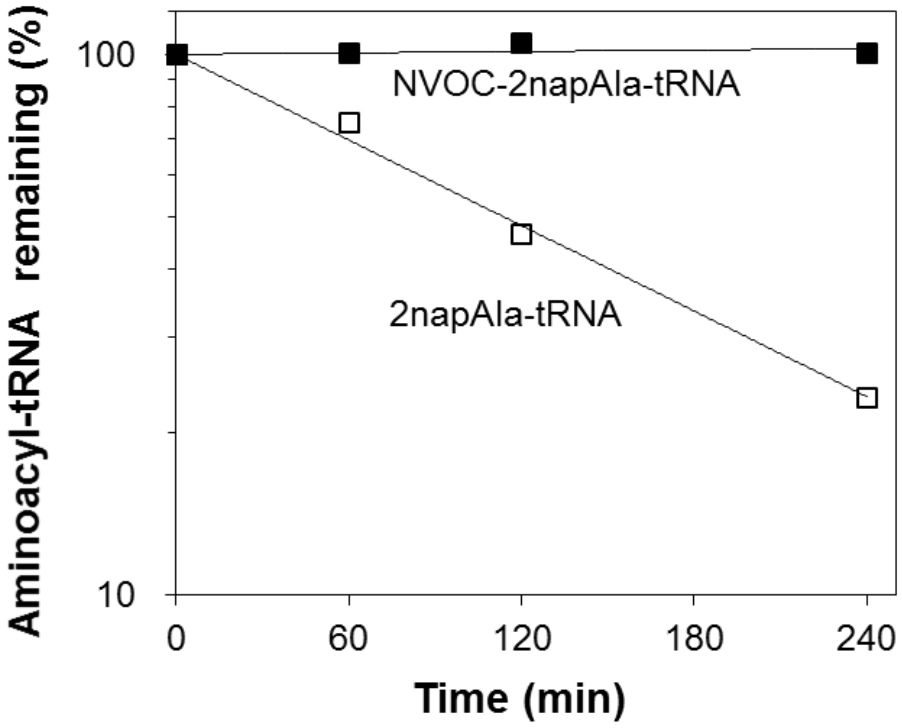

Figure 2-2. Deacylation profiles of 2napAla-tRNA and NVOC-2napAla-tRNA.

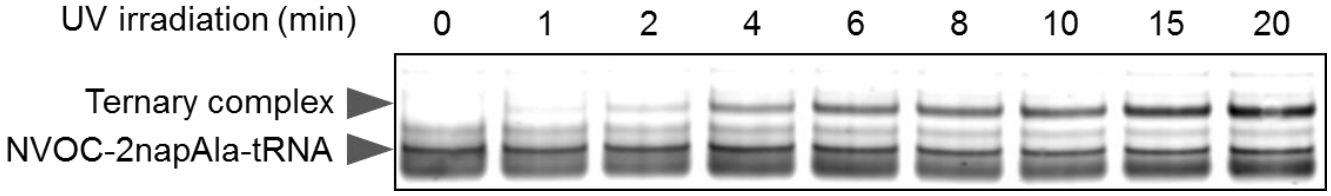

Figure 2-3. EF-Tu binding to the UV-irradiated NVOC-2napAla-tRNA. The ternary complex includes EF-Tu, GTP, and 2napAla-tRNA.

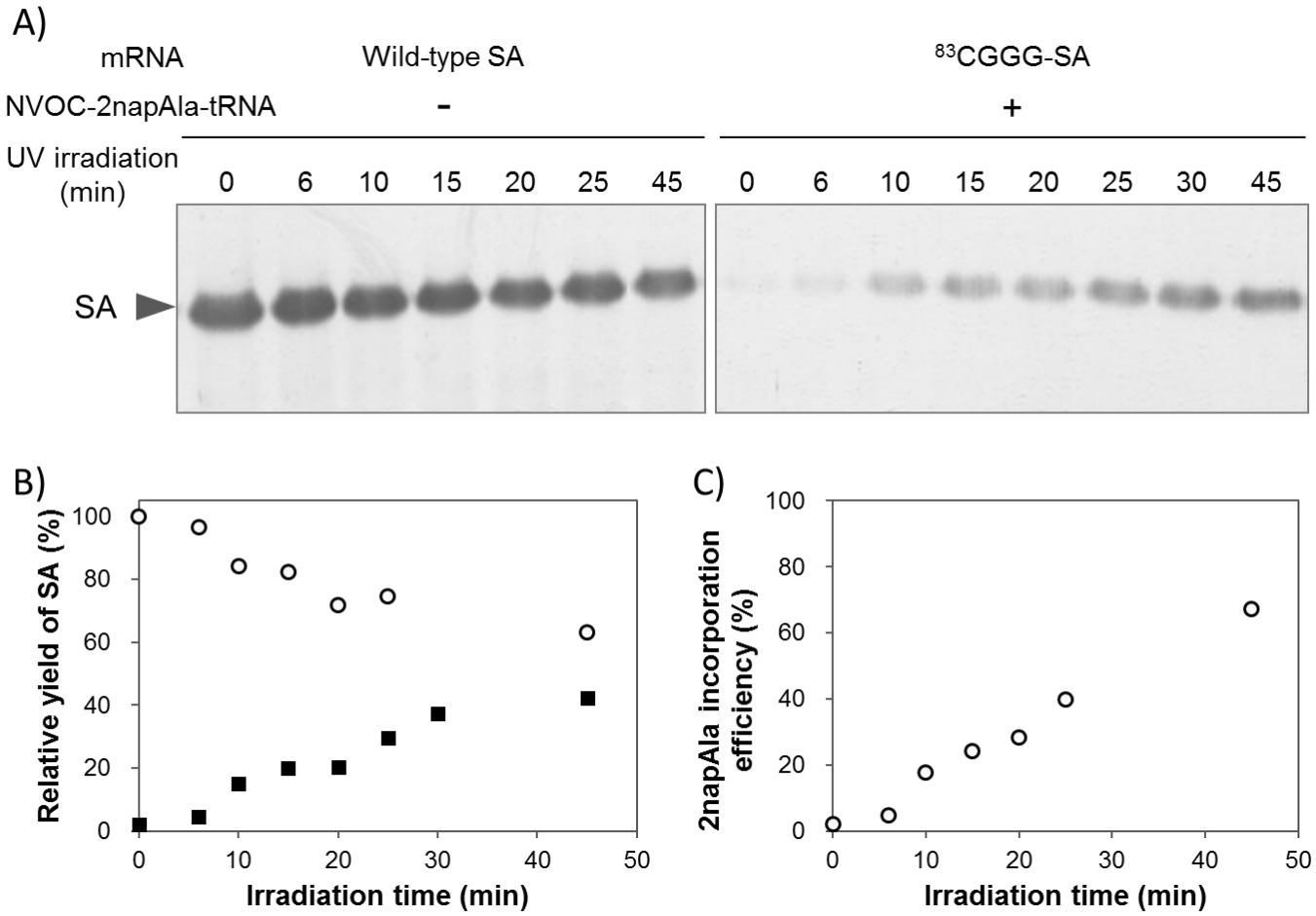

Figure 2-4. Light-dependent incorporation of 2napAla at the 83rd position of streptavidin protein using NVOC-2napAla-tRNA$_{CCCG}$. (A) Products obtained by translating wildtype SA mRNA (left) and those obtained by translating 83CGGG-SA mRNA with NVOC-2napAla-tRNA$_{CCCG}$ (right) were analyzed by Western blot. (B) Yield of SA protein relative to the product obtained by translating the wild-type mRNA without irradiation. Open circles show the yield of translation product from the wild-type SA mRNA. Filled squares show the yield of translation product from the

83CGGG-SA mRNA with NVOC-2napAla-tRNA$_{CCCG}$. (C) Efficiency of 2napAla incorporation into the 83rd position of SA relative to time of UV irradiation. The incorporation efficiencies were estimated considering the irradiation-time dependent decrease in translation efficiency.

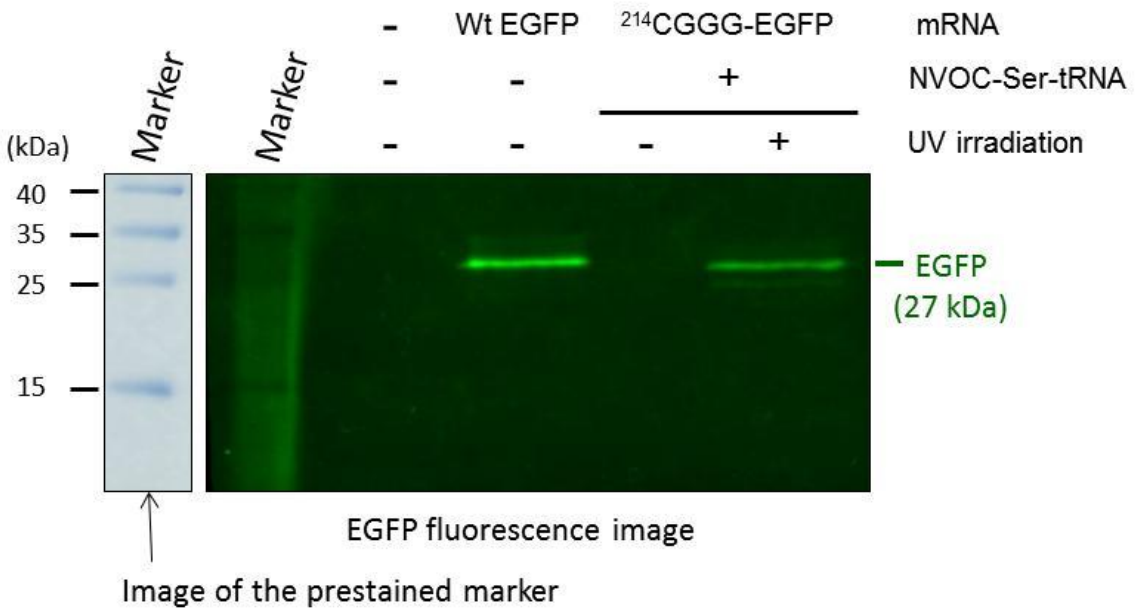

Figure 2-5. Light-dependent incorporation of serine at the 214th position of EGFP using NVOC-Ser-tRNA. The mutant EGFP mRNA with a CGGG codon position 214 was translated *in vitro* using NVOC-Ser-tRNA and loaded onto a 15% SDS-PAGE. The heat denaturation step was omitted to visualize EGFP fluorescence in the gel.

Conclusion

We have demonstrated photo-dependent protein synthesis using NVOC-aa-tRNAs with two kinds of mRNAs (SA and EGFP) and two kinds of amino acids (the non-natural amino acid 2napAla and the natural amino acid serine). This is the first report of light-dependent protein synthesis using caged aa-tRNAs. To avoid photo-damage to the protein biosynthesis system, caged compounds other than NVOC will be investigated in future. Caged compounds, which can be uncaged by visible light or more rapidly uncaged, may be more suitable for this application. The caged aa-tRNA will be tested for photo-regulation of translation in living cells and may prove applicable for synthetic biology and biomedical studies.

Reference

[1] Kawakami T and Murakami H 2012 *J. Nucleic Acids* **2012** 713510.

[2] Hohsaka T, Ashizuka Y, Murakami H and Sisido M 1996 *J. Am. Chem. Soc.* **118** 9778.

[3] Hohsaka T, Kajihara D, Ashizuka Y, Murakami H and Sisido M 1999 *J. Am. Chem. Soc.* **121** 34.

[4] Akahoshi A, Suzue Y, Kitamatsu M, Sisido M and Ohtsuki T 2011 *Biochem. Biophys. Res. Commun.* **414** 625.

[5] Kim CH, Axup JY and Schultz PG 2013 *Curr. Opin. Chem. Biol.* **17** 412.

[6] Le DD, Cortesi AT, Myers SA, Burlingame AL and Fujimori DG 2013 *J. Am. Chem. Soc.* **135** 2879.

[7] Kajihara D, Abe R, Iijima I, Komiyama C, Sisido M and Hohsaka T 2006 *Nat. Methods* **3** 923.

[8] Nakata H, Ohtsuki T and Sisido M 2009 *Anal. Biochem.* **390** 121.

[9] Ellis-Davies GCR 2007 *Nat. Methods* **4** 619.

[10] Ando H, Furuta T, Tsien RY and Okamoto H 2001 *Nat. Genet.* **28** 317.

[11] Ogasawara S and Maeda M 2011 *Bioorg. Med. Chem. Lett.* **21** 5457.

[12] Shah S, Rangarajan S and Friedman SH 2005 *Angew. Chem. Int. Ed. Engl.* **44** 1328.

[13] Mikat V and Heckel A 2007 *RNA* **13** 2341.

[14] Govan JM, Young DD, Lusic H, Liu Q, Lively MO and Deiters A 2013 *Nucleic Acids Res.* **41** 10518.

[15] Endoh T, Sisido M and Ohtsuki T 2008 *Bioconjug. Chem.* **19** 1017.

[16] Endoh T, Sisido M and Ohtsuki T 2009 *J. Control. Release* **137** 241.

[17] Matsushita-Ishiodori Y, Kuwabara R, Sakakoshi H, Endoh T and Ohtsuki T 2011 *Bioconjug. Chem.* **22** 2222.

[18] Matsushita-Ishiodori Y and Ohtsuki T 2012 *Acc. Chem. Res.* **45** 1039.

[19] Robertson SA, Ellman JA and Schultz PG 1991 *J. Am. Chem. Soc.* **113** 2722.

[20] Ohtsuki T, Manabe T and Sisido M 2005 *FEBS Lett.* **579** 6769.

[21] Sisido M, Ninomiya K, Ohtsuki T and Hohsaka T 2005 *Methods* **36** 270.

[22] Fluorescence intensity of 2napAla (λ_{ex} = 270 nm and λ_{em} = 334 nm) was monitored using a FLP-6600 spectrofluoro-photometer (Jasco). The fluorescence intensity of the NVOC-2napAla-pdCpA [2.5 μM, dissolved in 1 mM potassium acetate (KOAc), pH 5.0], was measured

after 5, 10, 15, 20, 30, 40, 50, and 60 min of UV irradiation at 365 nm using a UVL-56 Handheld UV Lamp (UVP) (5.67 mW/cm^2)

[23] McCray JA and Trentham DR 1989 *Annu. Rev. Biophys. Biophys. Chem.* **18** 239.

[23] Pingoud A, Urbanke C, Krauss G, Peters F and Maass G 1977 *Eur. J. Biochem.* **78** 403.

[24] Deacylation of NVOC-2napAla-tRNA and 2napAla-tRNA at 37°C in 25mM Hepes–KOH (pH 7.5) was monitored by acid PAGE analysis as follows. Aliquots (4 µL) of 10 µM aa-tRNA in 20 mM Hepes–KOH (pH 7.5) were incubated at 37°C. The solution was then mixed with equal volumes of acrylamide gel loading solution (200 mM NaOAc (pH 5.0), 20 mM EDTA, and 7 M urea). The samples were separated by 7.5% PAGE at 4°C and 500 V for 18 h in a buffer containing 100 mM NaOAc (pH 5.0) and 10 mM EDTA. The gels were stained with SYBR Gold (Invitrogen, USA), and the aa-tRNA (or NVOC-aa-tRNA) and deacylated tRNA were estimated from the band intensities using ImageJ (National Institutes of Health, U.S.A., http://rsb.info.nih.gov/ij/).

[26] Arita M, Suematsu T, Osanai A, Inaba T, Kamiya H, Kita K, Sisido M, Watanabe Y and Ohtsuki T 2006 *Nucleic Acids Res.* **34** 5291.

[27] Stepanov VG and Nyborg J 2002 *Extremophiles* **6** 485.

[28] Doi Y, Ohtsuki T, Shimizu Y, Ueda T and Sisido M 2007 *J. Am. Chem. Soc.* **129** 14458.

[29] Prior to the binding analysis, the NVOC-2napAla-tRNA was dissolved in 6 mM KOAc (pH 5.0) and irradiated at 4°C for 0–20 min using a UVL-56 Handheld UV Lamp. The ternary complex of EF-Tu, GTP, and aa-tRNA was prepared and analyzed on 8% polyacrylamide gels. Fluorescence of SYPRO Red-stained ternary complex bands were also measured on the FluoroMax-2 (HORIBA, Japan) (λ_{ex} = 405 nm and λ_{em} = 450–470 nm).

[30] The SA protein was synthesized in a 10 μL reaction mixture containing 55 mM Hepes–KOH (pH 7.5), 210 mM potassium glutamate, 6.9 mM NH_4OAc, 9 mM MgOAc, 1.7 mM DTT, 1.2 mM ATP, 0.28 mM GTP, 26 mM phosphoenolpyruvate, 1 mM spermidine, 1.9% polyethylene glycol-8000, 35 μg/mL folinic acid, an amino acid mixture containing 0.1 mM of each amino acid except arginine, 0.01 mM arginine, 8 μg SA mRNA, 2 μg NVOC- 2napAla-tRNA, and 2 μL *E. coli* S30 extract (Promega). The reaction mixture was first incubated at 4°C for 45 min. During the incubation, the reaction mixture was irradiated at 365 nm for 0–45 min. The reaction mixture was then incubated at 37°C for 60 min. The reaction mixtures, including synthesized proteins, were loaded

onto a 15% SDS–PAGE gel and analyzed by Western blotting. The band intensities of SA were calculated using the ImageJ software.

[31] Enhanced green fluorescent protein (EGFP) mRNA with a CGGG codon at the 214th amino acid position (214CGGG-EGFP mRNA) was prepared. We performed the *in vitro* translation in a 10 µl reaction mixture containing 55 mM Hepes-KOH (pH 7.5), 210 mM potassium glutamate, 6.9 mM NH4OAc, 9 mM MgOAc, 1.7 mM DTT, 1.2 mM ATP, 0.28 mM GTP, 26 mM phosphoenolpyruvate, 1 mM spermidine, 1.9% polyethylene glycol-8000, 35 µg/ml folinic acid, an amino acid mixture containing 0.1 mM of each amino acid except arginine, 0.01 mM arginine, 0.4 nmol EGFP mRNA, 0.1 nmol NVOC-Ser-tRNA, and 2 µl *E. coli* S30 extract (Promega). The reaction mixture was incubated at 37°C for 60 min after UV irradiation at 365 nm. The reaction mixture was loaded onto a 15% SDS-PAGE gel, and EGFP fluorescence was captured using an FLA-9000 imager (Fujifilm, Japan) with an λ_{ex}= 489 nm and λ_{em} = 508 nm. The fluorescence band intensities of EGFP were calculated using ImageJ.

Chapter 3

Enhanced Cellular Uptake of lactosome using Cell-Penetrating Peptides

Introduction

The use of nanoparticles as drug carriers for the selective delivery of pharmacological agents in various diseases such as cancer and viral infections has been studied [1, 2]. Over the past few decades, many nanoparticles, including liposomes [3], polymeric micelles [4, 5], metal nanoparticles [6], and dendrimers [7], have been developed for drug delivery. Among them, polymeric micelles are size-controllable and easily modified for adding new abilities, such as targeting and imaging. The polymers that comprise the micelles are size-controllable and can have various reactive groups. Several liposome drugs have been approved and are in clinical use, and polymeric micelles are in the clinical test phase [5, 8, 9].

Lactosomes are polymeric micelles composed of an amphipathic polymer with a hydrophilic poly(sarcosine) (PSar) block and a hydrophobic poly(L-lactic acid) (PLLA) block (AB-type) [10, 11]. The high density of PSar chains around the molecular assemblies contributes to their ability to escape from the reticuloendothelial system (RES) recognition, similarly to polyethylene glycol (PEG) modification [12]. Furthermore, PSar is considered to have an advantage over PEG in terms of biodegradability. AB-type lactosomes persist in the bloodstream for a long time [13]. However, AB-type lactosomes exhibit a drawback in multiple *in vivo* administrations [14], in which they accumulate in solid tumors after the first administration,

but accumulate only slightly after the second administration. To compensate for this drawback, a lactosome composed of $(PSar)_3$-block-PLLA (A_3B-type) has recently been developed [15]. The AB-type and A_3B-type lactosomes accumulate in tumor tissue through the enhanced permeation and retention (EPR) effect [16]. However, the lactosomes are not efficiently internalized by cells even if they accumulate around them. Improving the cellular uptake of the lactosomes is important for the efficient delivery of drugs that act intracellularly.

In this study, we attempted to modify A_3B-type lactosomes with cell-penetrating peptides (CPPs) to increase efficiency of their cellular uptake. CPPs are short peptides often rich in cationic residues, which have the ability to internalize various cargo molecules such as nucleic acids, proteins, and nanoparticles [17-19]. We used seven CPPs, including those derived from natural proteins (Tat and DPV3) [20-22] and chimeric or artificial peptides (PTD4, $MPG^{\Delta NLS}$, Pep1, and EB1) [23-26]. Cellular uptake efficiency of various CPP-modified lactosomes was compared. In addition, the photosensitizer 5,10,15,20-tetraphenyl-21*H*,23*H*-porphyrin (TPP) [27] was delivered to mammalian cells (including cancer cell lines) by the CPP-modified lactosomes. The cells were treated with the TPP-encapsulated lactosome and photoirradiated to evaluate the photodynamic therapy (PDT) effect. Finally, *in vivo* localization of the CPP-modified lactosomes was investigated using tumor-bearing mice.

Experimental details

Materials

$(PSar_{25})_3$-block-$PLLA_{35}$, indocyanine green (ICG)-$PLLA_{34}$, and maleimide-$PSar_{56}$-$PLLA_{30}$ were synthesized as described [11, 15, 28]. Chinese hamster ovary (CHO) cells (FLIP-In cell line) were purchased from Invitrogen (USA). NCI-N87 human gastric cancer cells and PANC-1 human pancreatic carcinoma cells were purchased from the American Type Culture Collection. The CPPs listed in Table 3-1 were prepared by Fmoc-based solid-phase peptide synthesis and provided by the Central Research Laboratory at the Okayama University Medical School.

Preparation of lactosome complexes

A chloroform solution containing the $(PSar_{25})_3$-block-$PLLA_{35}$ (100 nmol, 7.7 μg) with 4 mol% of TPP (Wako Pure Chemical, Japan), 2 mol% of ICG-$PLLA_{34}$, and 10 mol% maleimide-$PSar_{56}$-$PLLA_{30}$ was evaporated under reduced pressure to remove the solvent, forming a thin film on the surface of the glass test tube. Saline (Otsuka normal saline, Otsuka Pharmaceutical Factory, Japan) (50 μL) was added to the test tube, which was then placed at room temperature for 5 min. Then, 50 μL of the saline solution containing 50 nmol CPP and 10 nmol Tris(2-carboxyethyl)phosphine hydrochloride (Nacalai Tesque, Japan) were added

to the solution (50 μL) in the test tube and stirred for 12 h at room temperature. In this procedure, lactosome formation and TPP encapsulation by the lactosome were expected. At the same time, maleimide-$PSar_{56}$-$PLLA_{30}$ in the lactosome is expected to react with CPP, which contains a cysteine residue at its C-terminus (Table 3-1). This lactosome mixture was diluted with 400 μL of saline, and passed through a 0.1 μm syringe filter (Membrane Solutions, USA) to remove large aggregates. Low molecular weight molecules were excluded from the mixture using Amicon Ultra-0.5 (MWCO 50 kDa, Merck Millipore, Germany). To analyze concentrations of CPP, TPP and ICG-$PLLA_{34}$, absorption spectra of the lactosome complexes were measured using a BioSpec spectrometer (Shimadzu, Japan). The particle size, size distribution, polydispersity index (PDI), and zeta potential were measured by Zetasizer Nano ZSP (Malvern Instruments, UK).

Analysis of lactosome complexes using size exclusion chromatography

Size exclusion chromatography was performed using a Superdex 200 10/300 GL column (GE Healthcare) on an HPLC system (Shimadzu). The mobile phase was 10 mM Tris-HCl (pH 7.4) at a flow rate of 0.5 mL/min. Absorbance was measured at 230, 280, 417, and 700 nm.

Detection of photogenerated singlet oxygen

Singlet oxygen ($^1O_2$) generation from the lactosome complexes (±TPP) was measured using singlet oxygen sensor green (SOSG) (Molecular Probes, USA). In a 96-well black plate with a clear bottom, 5 μL of the TPP-encapsulated lactosomes containing 1 μM TPP were mixed with 1 μL of 50 μM SOSG and diluted with 50 μL of distilled water. The lactosome solution was irradiated at 400–440 nm and 200 mW/cm^2 for 50 s (10 J/cm^2). Fluorescence intensity was measured at an excitation wavelength of 488 nm and an emission wavelength of 500–700 nm using a Jasco FP-6600 spectrofluorometer.

Evaluation of cellular uptake of the lactosome complexes containing CPPs

CHO cells were cultured at 37°C under 5% CO_2 in Ham's F12 medium (Wako Pure Chemical) supplemented with 10% FBS (Nichirei Biosciences, Japan), 100 units/mL penicillin (Gibco; Thermo Fisher Scientific, USA), and 100 μg/mL streptomycin (Gibco; Thermo Fisher Scientific). The cells were seeded at a density of 2×10^4 cells/well in the 96-well plate, and incubated at 37°C under 5% CO_2 overnight. The cells were then incubated at 37°C for 2 h with ICG-labeled lactosomes modified with CPPs (Tat, PTD4, DPV3, MPG$^{\Delta NLS}$, R9MPG, Pep1, or EB1) dissolved in 200 μL T buffer. The lactosome solution was exchanged for Ham's F12

medium before the fluorescence imaging. The cellular fluorescence images were obtained by fluorescence microscopy using an Olympus IX71 microscope with a 40× objective lens and a U-DM-CY7-3 mirror unit.

LysoTracker Green (Thermo Fisher Scientific, USA) was used for investigating cellular localization of CPP-modified lactosomes. After incubation of the cells with CPP-modified ICG-labeled lactosomes, the lactosome solution was exchanged with Ham's F12 medium containing 2 μM LysoTracker Green. The cells were further incubated for 3 h. Then, the cell medium was replaced with Ham's F12 medium, and fluorescence images were obtained.

To evaluate the cellular uptake of the lactosome complexes, the NIR fluorescence images were obtained using an IVIS spectrum system (Xenogen, USA) with a filter set specific for ICG (excitation at 745 nm and emission at 840±10 nm). The ICG fluorescence intensity was estimated from the photon counts of the images. Then, the cell medium was replaced with solution containing 10 μL of Cell Counting Kit-8 solution (Dojindo, Japan) and 90 μL of Ham's F12 medium, and the cells were incubated for an additional 1.5 h. After incubation, the cell viability was measured by absorbance at 450 nm using the microplate reader SunriseR (Tecan Japan, Japan). Lactosome uptake levels were calculated by dividing ICG fluorescence intensity by cell viability of each well.

Measurement of cell viability after treatment with the TPP-loaded lactosomes and light

NCI-N87 cells were cultured at 37°C under 5% CO_2 in RPMI1640 medium (Wako Pure Chemical) supplemented with 10% FBS, 100 units/mL penicillin, and 100 μg/mL streptomycin. NCI-N87 cells were seeded at a density of 4×10^4 cells/well in a 96-well plate, and incubated at 37°C for 2 d before treatment with the lactosome complex. The effect of treatment with the TPP-loaded lactosomes and light on cell viability, which is related to PDT efficacy, was evaluated as follows: TPP-loaded lactosomes modified with CPPs (Pep1, EB1, or DPV3) dissolved in 200 μL of T buffer (20 mM HEPES-KOH (pH 7.4), 115 mM NaCl, 5.4 mM KCl, 1.8 mM $CaCl_2$, 0.8 mM $MgCl_2$, and 13.8 mM glucose) were added to NCI-N87 cells (70% confluent) in the 96-well plate. The cells were incubated at 37°C for 1.5 h. After the lactosome solution was exchanged for T buffer, the cells were irradiated at 340–390 nm at 200 mW/cm^2 for 100 s. After irradiation, the cells were further incubated for 24 h at 37°C under 5% CO_2 in the RPMI1640 medium. Then, the cell medium was exchanged for the solution containing 10 μL of Cell Counting Kit-8 solution and 90 μL of RPMI1640 medium, and the cells were incubated at 37°C for 2 h. The cell viability was measured by the absorbance at 450 nm using a microplate reader SunriseR. Statistical analysis was performed with EZR (Saitama Medical Center, Japan) using one-way ANOVA followed by Dunnett's test.

Tumor-bearing mice and in vivo *imaging*

Six-week-old male nude mice (BALB/c nu/nu) were purchased from Charles River. Five weeks before the imaging, PANC-1 cells (1×10^7) suspended in 100 μL of 50% Matrigel Matrix (Corning Life Sciences, USA) in PBS was subcutaneously inoculated into the front left leg of mice. Two weeks after the first transplantation, NCI-N87 cells (4×10^6) were suspended in the Matrigel solution and subcutaneously inoculated into the front right leg of mice. Three weeks after the second transplantation, CPP/TPP/ICG-lactosomes were injected into the tumor-bearing mouse via the tail vein. After 24 h, ICG fluorescence images were taken using the IVIS spectrum system (excitation at 745 nm and emission at 840±10 nm, field of view=12.5 cm (width and height), f/stop = 2, binning = 4, and exposure time at 3 s). During the imaging process, the mice were anesthetized using 3.0% isoflurane gas in oxygen flow (0.5 L/min).

Results and Discussions

Characterization of the CPP-modified lactosomes

The particle sizes of lactosome complexes were measured by dynamic light scattering (DLS). The average particle sizes of the CPP-modified lactosomes were 36–49 nm, which were slightly larger than the unmodified lactosomes (34.2 nm) (Table 3-2, Fig. 3-1b). The zeta potential value of CPP-modified lactosomes (e.g., Pep1-modified lactosome: 1.74 mV, EB1-modified lactosome: 1.60 mV) was higher than that of the unmodified lactosomes (-4.60 mV) (Table 3-2). The increase in the zeta potential seems to be due to positively charged CPPs. These results indicated that modification of lactosomes with CPPs increased their surface charge and particle size. To confirm the incorporation of the CPP (EB1), TPP, and ICG-PLLA into the lactosomes, size exclusion chromatography was performed using a Superdex 200 10/300 GL column and the HPLC system (Fig. 3-1c-g). The purified lactosome complex containing EB1, TPP, and ICG (EB1/TPP/ICG-lactosome) was eluted as a single peak from the column, and its retention time was the same as in the unmodified lactosomes (Fig. 3-1c, d). Absorbance traces of the chromatography at 230 nm, 280 nm, 417 nm, and 700 nm suggested that EB1, TPP, and ICG-PLLA were successfully incorporated into lactosome complexes (Fig. 3-1c-g). EB1 is thought to bind to maleimide-$PSar_{56}$-$PLLA_{30}$ in the lactosome, and TPP is thought to be

encapsulated in the hydrophobic core of the lactosome by hydrophobic interaction.

Cellular uptake of CPP-modified lactosomes

Internalization of CPP-modified lactosomes by CHO cells was observed by fluorescence microscopy (Fig. 3-2a). ICG-labeled CPP-modified lactosomes were added to CHO cells and incubated at 37°C for 2 h. After the incubation and washing steps, significantly strong ICG fluorescence was observed in the CHO cells treated with the Pep1- and EB1-modified lactosomes, compared to the lactosomes without CPP. The CPP-modified lactosomes showed dotted localization. Pep1- and EB1-modified lactosomes co-localized with LysoTracker Green (Fig. 3-2b), indicating that they localized mainly in acidic organelles, including endosomes and lysosomes. Furthermore, the lactosome uptake level of the cells was estimated from the ICG fluorescence intensity and cell viability of each culture well (Fig. 3-2c). The EB1-modified lactosomes was the most abundantly internalized by the cells. Pep1-modified lactosomes were also highly internalized (their uptake level relative to the EB1-modified lactosomes was 0.62). These results indicated that cellular uptake of lactosomes was improved by the addition of CPPs, especially EB1 and Pep1. These results showed that cellular uptake efficiency of the lactosomes

modified with amphipathic CPPs was higher than that of lactosomes modified with non-amphipathic CPPs, which may related to the binding efficiency of the CPPs to lactosomes. There was no relationship between the size of the CPP-modified lactosomes (Table 3-2) and the cellular uptake efficiency. Zeta potential seems to be related to the cellular uptake efficiency because both EB1- and Pep1-modified lactosomes had positive zeta potential (Table 3-2), while the others had negative potential.

Singlet oxygen generation from TPP-loaded lactosome

PDT with the use of a photosensitizer is generally based on photoinduced singlet oxygen generation from the photosensitizer. TPP encapsulated in lactosomes may lose its photosensitizing ability. Thus, we confirmed singlet oxygen generation from TPP-loaded lactosomes using the singlet oxygen indicator SOSG. Figure 3-3 indicates that singlet oxygen was photo-dependently generated from TPP-loaded lactosomes. Therefore, this lactosome complex can be applied for PDT.

Photoinduced cell killing efficacy of the CPP-modified TPP-loaded lactosomes

Cell treatment with a photosensitizer and light is called PDT treatment and can be used for killing malignant or cancer cells. To evaluate the effect of PDT treatment using the CPP-modified and TPP-loaded lactosomes (CPP/TPP-lactosomes), cell viability was measured after treatment with CPP/TPP-lactosomes followed by photoirradiation, and 24 h culture in the medium. EB1/TPP-lactosomes and Pep1/TPP-lactosomes with photoirradiation efficiently induced the killing of NCI-N87 cells (89% and 67%, respectively, compared to the experiment without CPP/TPP-lactosomes) (Fig. 3-4a). Similar results were obtained in CHO cells (Fig. 3-4b). The cell damage observed with these CPP/TPP-lactosomes is thought to be due to the photo-generated singlet oxygen (Figure 3-3). The efficiency of the cell killing was related to the cellular uptake efficiency of CPP-modified lactosomes (Fig. 3-2) (EB1 > Pep1 > other CPPs). These results indicated that the EB1 peptide was the most effective CPP for cellular internalization of TPP lactosomes.

In vivo *imaging*

To confirm the accumulation of EB1/TPP/ICG-lactosomes in tumor sites, lactosomes were administrated to mice bearing NCI-N87 and PANC-1 tumors, and ICG fluorescence images were obtained. Reproducibility was confirmed using three mice, and the representative image is shown in Figure 3-5. Twenty-four hours after injection, ICG fluorescence was detected in the NCI-N87 tumor, indicating that the EB1-modified lactosome accumulated in NCI-N87 tumors (Fig. 3-5a), though it accumulated less than the lactosome lacking the CPP (Fig. 3-5b). In contrast, only slight ICG fluorescence was detected in the PANC-1 tumor. These observations are consistent with those of the previous reports [28, 29]. The accumulation of lactosomes in NCI-N87 tumors has also been reported in a study that used HER2-modified AB-type lactosomes [28]. Pancreatic tumors are known to be poorly permeable, and among polymeric micelles with diameters of 30, 50, 70, and 100 nm, only the 30 nm micelles accumulated in pancreatic tumors [29]. Since the size of the EB1-modified lactosomes used in this study was ~38 nm, reducing the size of the CPP-modified lactosomes may increase their accumulation in tumors.

Table 3-1. Cell-penetrating peptides used in this study.

CPP	Classification	Length	Sequence
Tat	Cationic	11	YGRKKRRQRRR-C
PTD4	Cationic	11	YARAAARQARA-C
DPV3	Cationic	16	RKKRRRESRKKRRRES-C
$MPG^{\Delta NLS}$	Amphipathic	27	GALFLGFLGAAGSTMGAWSQPKSKRKV-C
R9MPG	Amphipathic	25	RRRRRRRRRGALFLAFLAAALSLMG-C
Pep1	Amphipathic	21	KETWWETWWTEWSQPKKKRKV-C
EB1	Amphipathic	23	LIRLWSHLIHIWFQNRRLKWKKK-C

Table 3-2. Particle size and zeta potential of CPP-modified lactosomes

CPP	Size (nm)	Zeta potential (mV)	PDI
-CPP	34.2±0.497	-4.60±0.225	0.134±0.007
Tat	36.2±0.250	-3.58±0.113	0.103±0.008
PTD4	37.0±0.367	-4.22±0.340	0.139±0.015
DPV3	37.0±0.400	-3.65±0.275	0.120±0.008
$MPG^{\Delta NLS}$	49.1±0.537	-2.93±0.641	0.287±0.022
R9MPG	43.9±1.531	-2.69±0.872	0.219±0.014
Pep1	37.7±0.618	1.74±0.061	0.126±0.017
EB1	38.3±0.182	1.60±0.316	0.117±0.010

These data were determined by DLS and laser Doppler electrophoresis (n = 3, mean ± standard deviation).

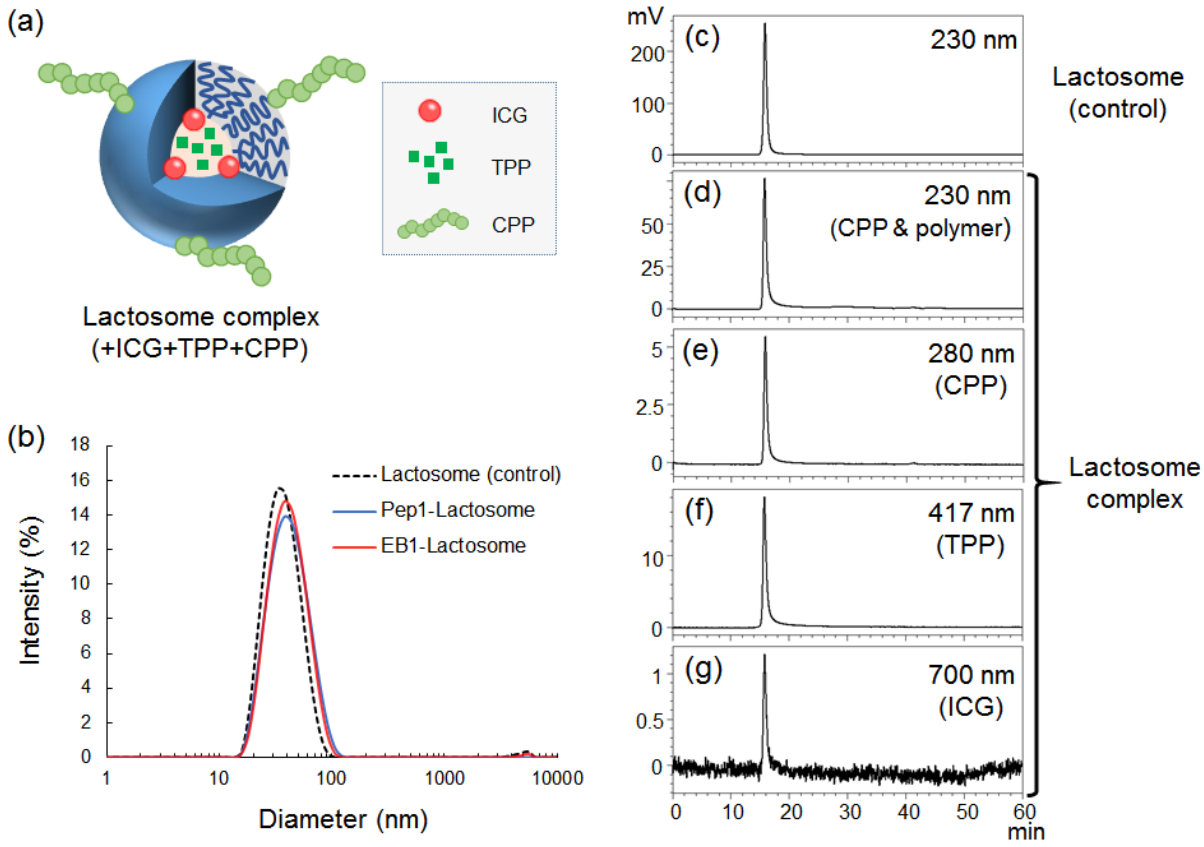

Figure 3-1. Characterization of lactosome complexes. (a) A diagram of the lactosome complex. (b) Size distribution of lactosomes modified with Pep1 or EB1 peptide. (c-g) Size exclusion chromatography of (c) unmodified and (d-g) EB1/TPP/ICG-lactosomes. Absorbance traces at (c, d) 230 nm, (e) 280 nm, (f) 417 nm, and (g) 700 nm.

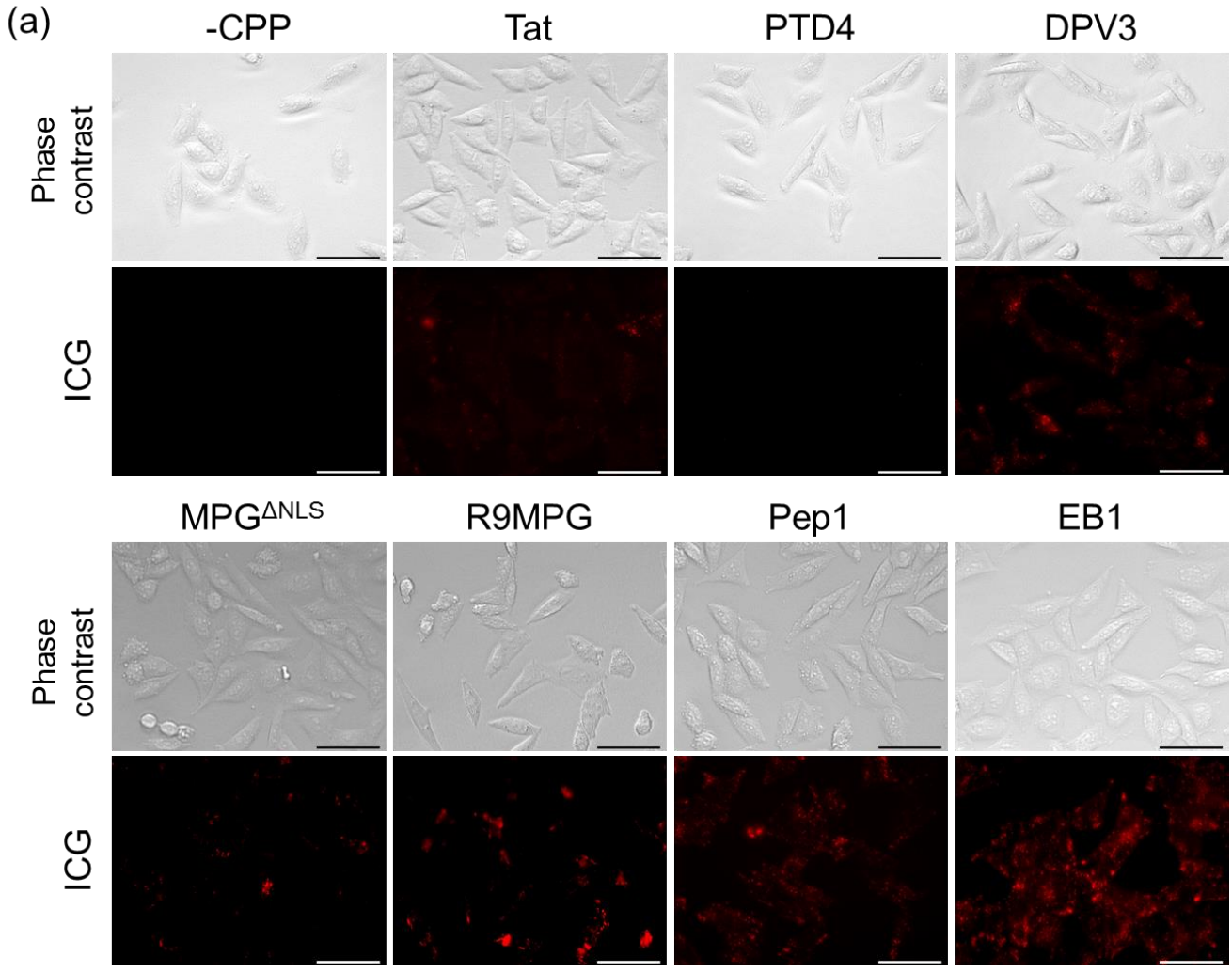
(a)
-CPP
Tat
PTD4
DPV3
Phase contrast
ICG
MPGΔNLS
R9MPG
Pep1
EB1
Phase contrast
ICG

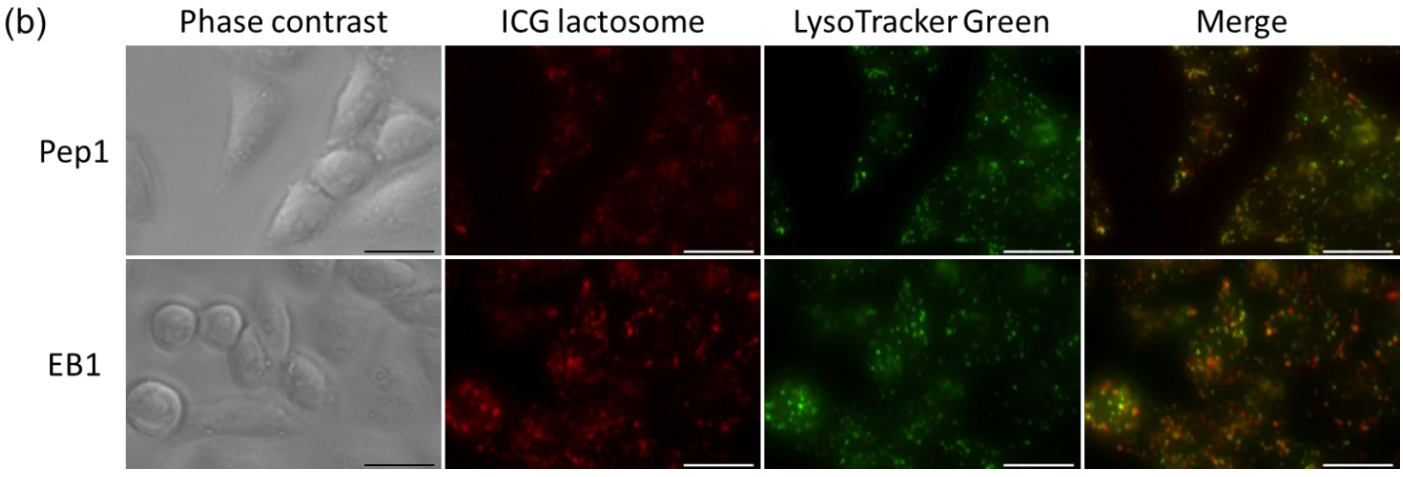
(b)
Phase contrast
ICG lactosome
LysoTracker Green
Merge
Pep1
EB1

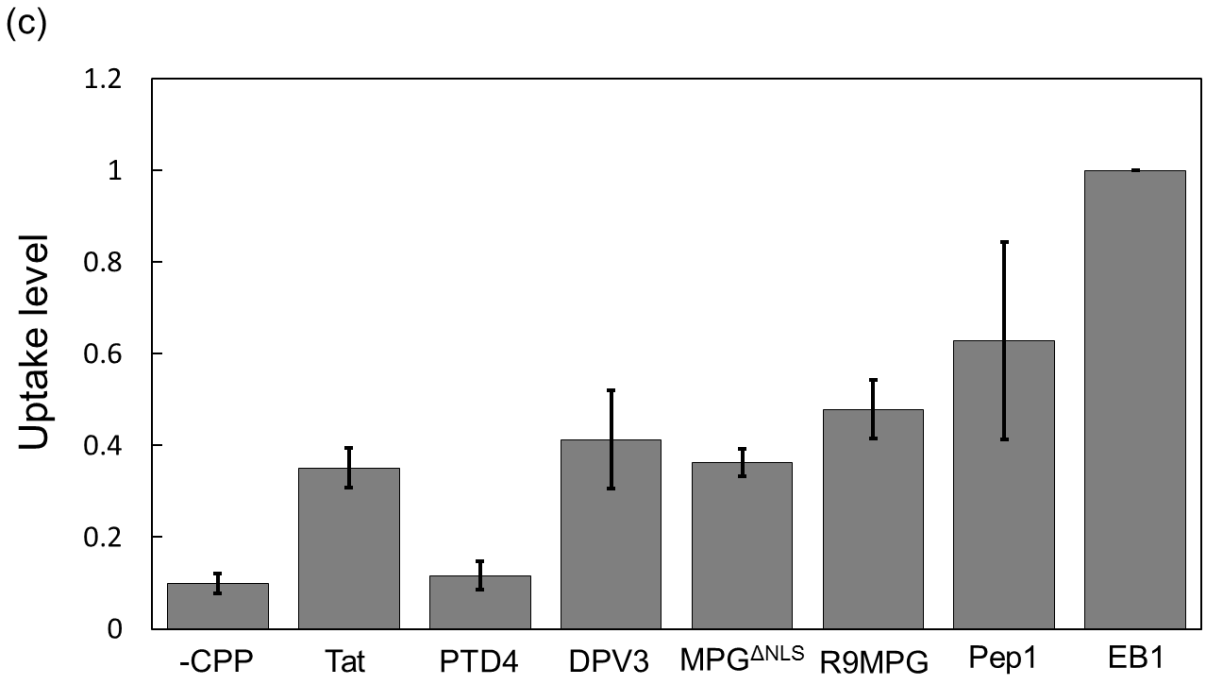

Fig. 3-2. Cellular uptake of the ICG-labeled lactosomes modified with CPPs (Tat, PTD4, DPV3, $MPG^{\Delta NLS}$, R9MPG, Pep1, or EB1). CHO cells were cultured with the lactosome complexes for 2 h at 37°C. (a) Microscope images of the cells cultured with the ICG-labeled and CPP-modified lactosomes. Scale bars represent 50 μm. (b) Images of Pep1- and EB1-modified ICG-lactosomes in the cells co-stained with LysoTracker Green. Scale bars indicate 20 μm. (c) Cellular uptake level calculated by dividing ICG fluorescence intensity by cell viability relative to that of the EB1-modified lactosomes. Values are expressed as mean ± standard error of the mean, n = 4.

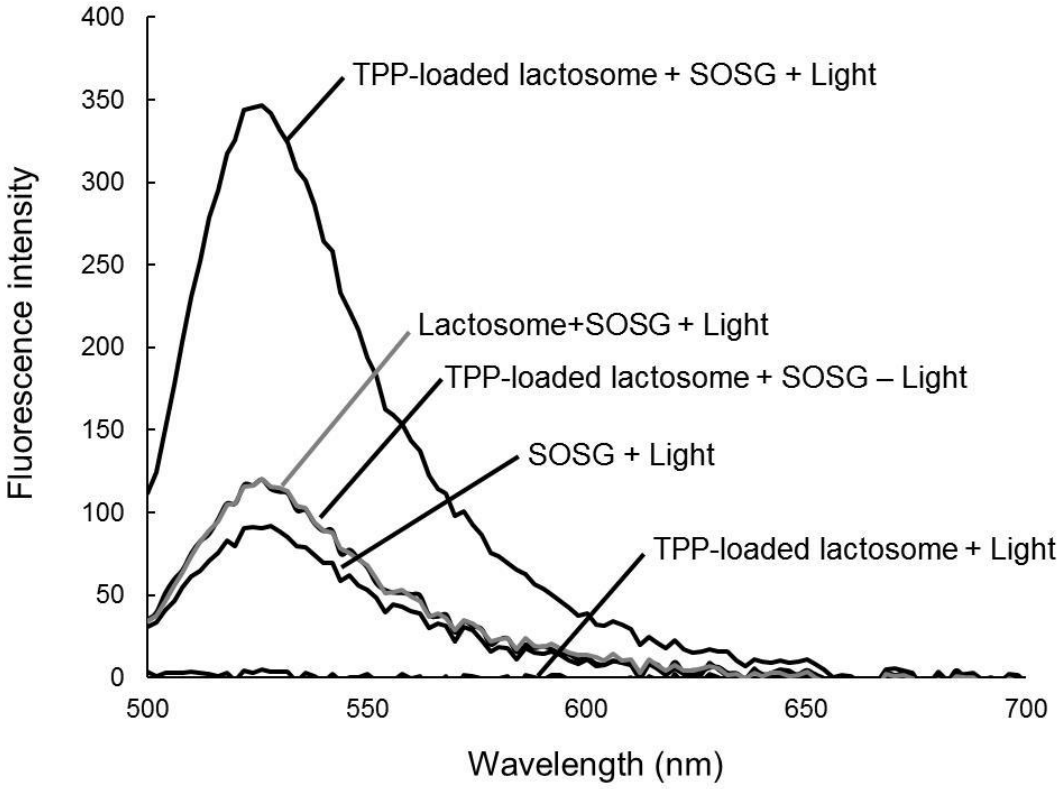

Figure 3-3. Fluorescence spectra of the SOSG with TPP-loaded or unloaded lactosomes after photoirradiation at 400-440 nm at 200 mW/cm^2 for 50 s. The excitation wavelength was 488 nm.

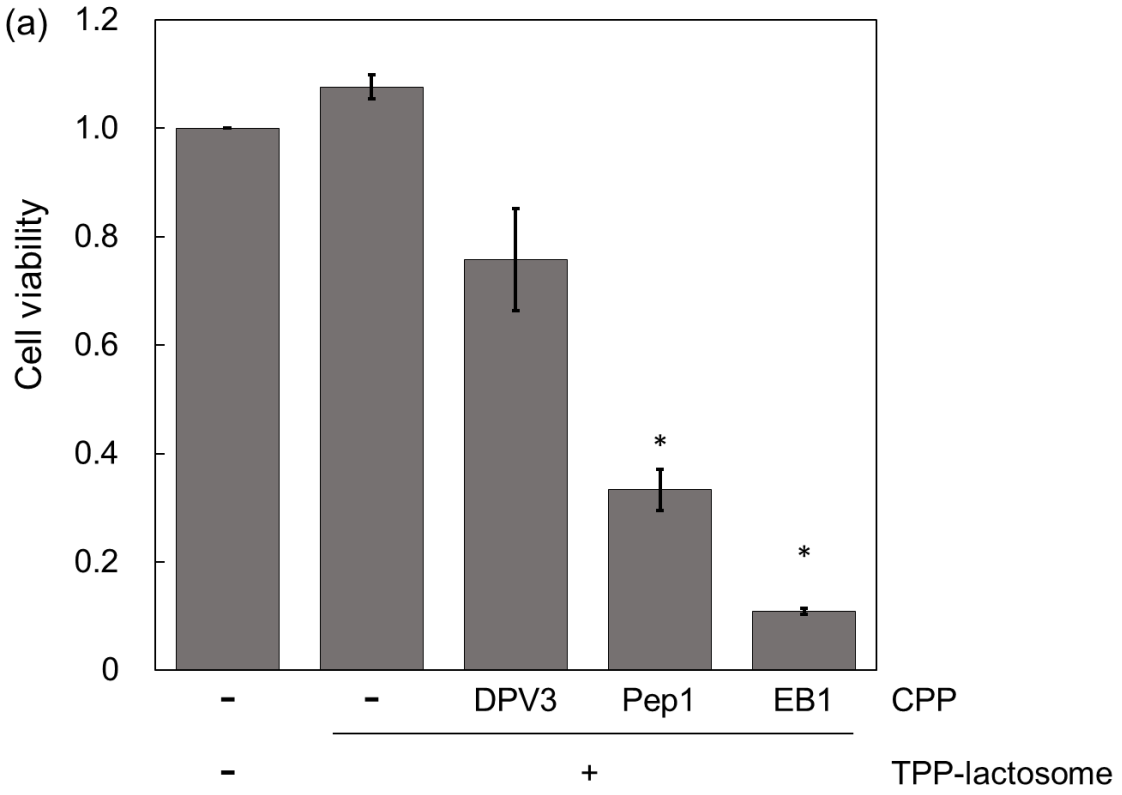
(a)
Cell viability
1.2
1.0
0.8
0.6
0.4
0.2
0
*
*
-
-
DPV3
Pep1
EB1
CPP
-
+
TPP-lactosome

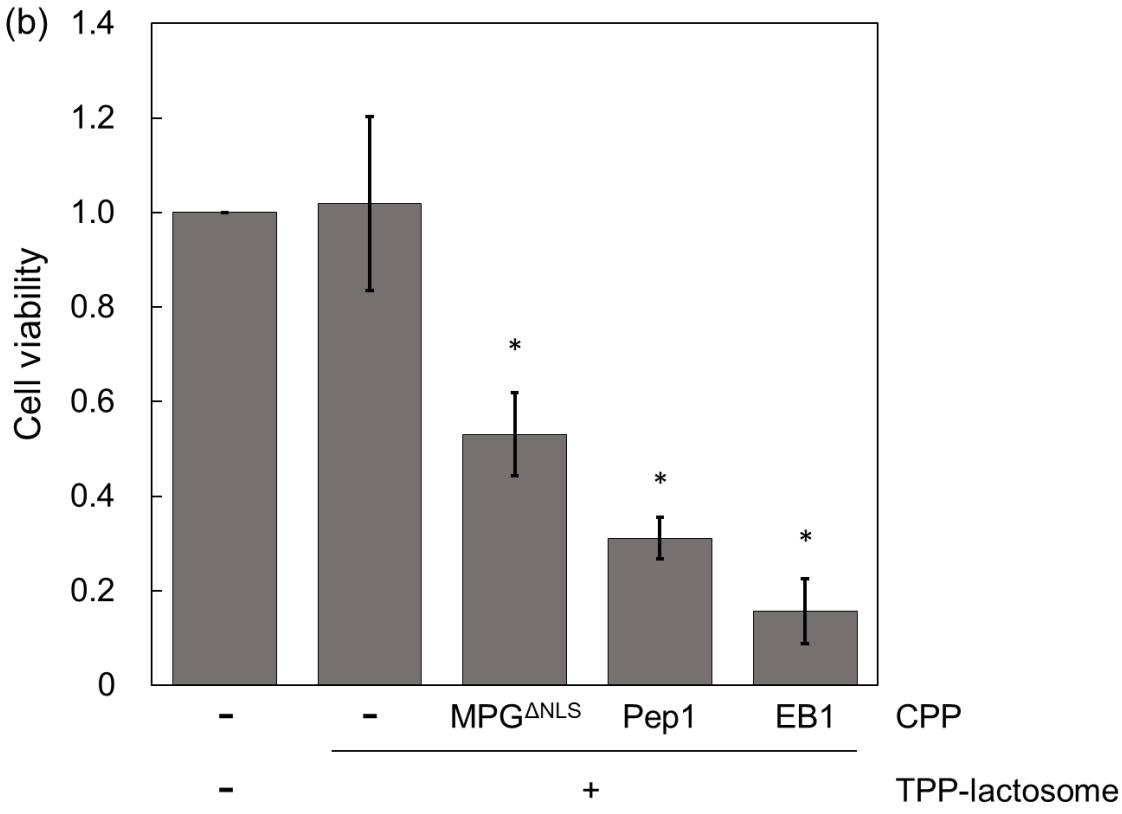
(b)
Cell viability
1.4
1.2
1.0
0.8
0.6
0.4
0.2
0
*
*
*
-
-
MPGΔNLS
Pep1
EB1
CPP
-
+
TPP-lactosome

Figure 3-4. Efficacy of the PDT treatment in (a) NCI-N87 cells and (b) CHO cells. After exposing the cells to CPP/TPP-lactosomes and light at wavelength of 340-390 nm at 200 mW/cm^2 for 100 s, cell viability was measured using the Cell Counting Kit-8. Cell viability values were normalized to that of untreated cells (- CPP, - TPP-lactosome), which were irradiated under conditions similar to the cells treated with CPP-lactosomes. Values are expressed as the mean ± standard error of the mean, n = 3. *P < 0.001 versus the untreated cells.

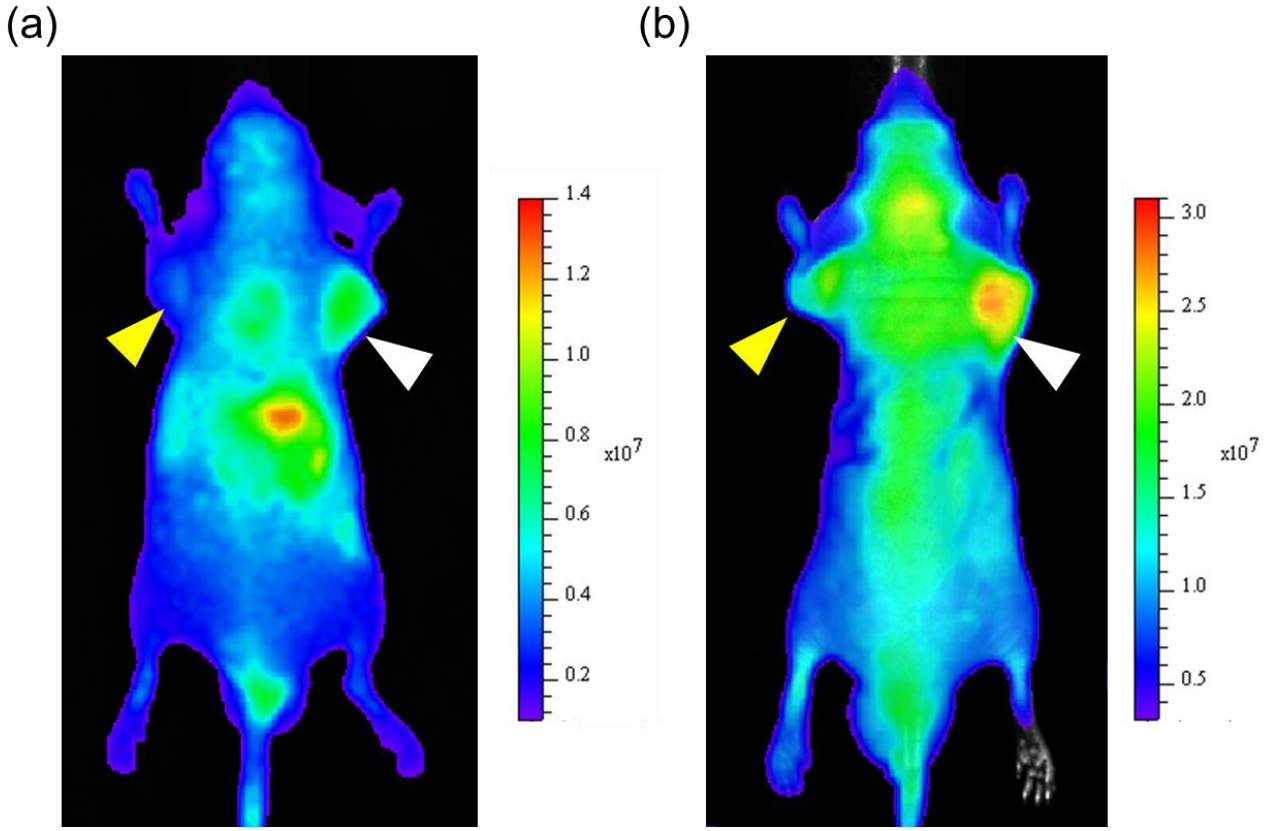

Figure 3-5. *In vivo* cancer imaging of CPP/TPP/ICG-lactosomes (a) TPP/ICG-lactosome (b). Ten-week-old male BALB/c nu/nu mice, grafting NCI-N87 and PANC-1 at front legs (right; NCI-N87, left; PANC-1) were used. The ICG image was obtained at 24 h after administration of the lactosomes to the tumor-bearing mouse. Arrows indicate tumor sites (white; NCI-N87, and yellow; PANC-1). The color bar indicates the fluorescence radiant efficiency (photons s^{-1} cm^{-2} $steradian^{-1}$).

Conclusions

The A_3B-type lactosome, a biocompatible and biodegradable polymeric nanomicelle, was modified with CPPs to improve its cellular uptake. Among the seven kinds of CPPs (Tat, PTD4, DPV3, $MPG^{\Delta NLS}$, R9MPG, Pep1, and EB1), amphipathic EB1 and Pep1 peptides greatly improved the uptake efficiency of the lactosomes. The CPP-modified lactosomes internalized by cells were localized mainly in endosomes or acidic organelles. We also conducted PDT experiments using the CPP-modified and photosensitizer-loaded lactosomes. Cell killing was efficiently photoinduced using the EB1/TPP and Pep1/TPP lactosomes. *In vivo* imaging of the EB1/TPP/ICG-lactosomes showed that they accumulated in NCI-N87 tumors in mice. More efficient tumor accumulation may be accomplished through the size-control of the CPP-modified lactosomes. The CPP-modified lactosome is promising as an efficient drug carrier. This study demonstrated that CPP-modified lactosomes encapsulated the hydrophobic agent TPP and delivered it into cells. Thus, CPP-modified lactosomes can deliver hydrophobic agents into cells. These lactosomes may also be able to deliver hydrophilic drugs such as proteins and nucleic acids into cells by attaching hydrophobic modifications to them.

Reference

[1] Durymanov MO, Rosenkranz AA and Sobolev AS 2015 *Theranostics* **5** 1007.

[2] Ndeboko B, Lemamy GJ, Nielsen PE and Cova L 2015 *Int. J. Mol. Sci.* **16** 28230.

[3] Allen TM and Cullis PR 2013 *Adv. Drug Deliv. Rev.* **65** 36.

[4] Deng C, Jiang Y, Cheng R, Meng F and Zhong Z 2012 *Nano Today* **7** 467.

[5] Cabral H and Kataoka K 2014 *J. Control. Release* **190** 465.

[6] Arvizo RR, Bhattacharyya S, Kudgus RA, Giri K, Bhattacharya R and Mukherjee P 2012 *Chem. Soc. Rev.* **41** 2943.

[7] Kesharwani P, Jain K and Jain NK 2014 *Prog. Polym. Sci.* **39** 268.

[8] Sanna V, Pala N and Sechi M 2014 *Int. J. Nanomedicine* **9** 467.

[9] Wicki A, Witzigmann D, Balasubramanian V and Huwyler J 2015 *J. Control. Release* **200** 138.

[10] Makino A, Yamahara R, Ozeki E and Kimura S 2007 *Chem. Lett.* **36** 1220.

[11] Makino A, Kizaka-Kondoh S, Yamahara R, Hara I, Kanzaki T, Ozeki E, Hiraoka M and Kimura S 2009 *Biomaterials* **30** 5156.

[12] Tanisaka H, Kizaka-Kondoh S, Makino A, Tanaka S, Hiraoka M and Kimura S 2008 *Bioconjug. Chem.* **19** 109.

[13] Makino A, Hara E, Hara I, Yamahara R, Kurihara K, Ozeki E, Yamamoto F and Kimura S 2012 *J. Control. Release* **161** 821.

[14] Hara E, Makino A, Kurihara K, Yamamoto F, Ozeki E and Kimura S 2012 *Int. Immunopharmacol.* **14** 261.

[15] Hara E, Ueda M, Makino A, Hara I, Ozeki E and Kimura S 2014 *ACS Med. Chem. Lett.* **5** 873.

[16] Matsumura Y and Maeda H 1986 *Cancer Res.* **46** 6387.

[17] Wang F, Wang Y, Zhang X, Zhang W, Guo S and Jin F 2014 *J. Control. Release* **174** 126.

[18] Copolovici DM, Langel K, Eriste E and Langel U 2014 *ACS Nano* **8** 1972.

[19] Endoh T and Ohtsuki T 2009 *Adv. Drug Deliv. Rev.* **61** 704.

[20] Frankel AD and Pabo CO 1988 *Cell* **55** 1189.

[21] Vives E, Brodin P and Lebleu B 1997 *J. Biol. Chem.* **272** 16010.

[22] De Coupade C, et al. 2005 *Biochem. J.* **390** 407.

[23] Ho A, Schwarze SR, Mermelstein SJ, Waksman G and Dowdy SF 2001 *Cancer Res.* **61** 474.

[24] Simeoni F, Morris MC, Heitz F and Divita G 2003 *Nucleic Acids Res.* **31** 2717.

[25] Morris MC, Depollier J, Mery J, Heitz F and Divita G 2001 *Nat. Biotechnol.* **19** 1173.

[26] Lundberg P, El-Andaloussi S, Sutlu T, Johansson H and Langel U 2007 *FASEB J.* **21** 2664.

[27] Canete M, Villanueva A, Dominguez V, Polo S, Juarranz A and Stockert JC 1998 *Int. J. Oncol.* **13** 497.

[28] Shimizu Y, Temma T, Hara I, Makino A, Yamahara R, Ozeki E, Ono M and Saji H 2014 *Nanomedicine* **10** 187.

[29] Cabral H, et al. 2011 *Nat. Nanotechnol.* **6** 815.

List of Publications

[1] Akiya Akahoshi, Yoshio Doi, Masahiko Sisido, Kazunori Watanabe, Takashi Ohtsuki

“Photo-dependent protein biosynthesis using a caged aminoacyl-tRNA”

BIOORGANIC & MEDICINAL CHEMISTRY LETTERS, Vol.24, No.23, pp.5369-5372 (2014)

[2] Akiya Akahoshi, Eiji Matuura, Eiichi Ozeki, Kazunori Watanabe and Takashi Ohtsuki.

“Enhanced cellular uptake of lactosome using cell-penetrating peptides”

I will submit a paper to *Journal of Science and Technology of Advanced Materials* with this title.

Acknowledgements

This study was carried out at the Department of Bioscience and Biotechnology, Graduate school of Natural Science and Technology, Okayama University under the supervision of Professor Dr. Takashi Ohtsuki during 2013 to 2016. I express sincere thanks for his kind and long-standing guidance, and encouragement throughout the present study.

I am sincerely grateful to Assistant Professor Dr. Kazunori Watanabe for his useful advice and discussions in detail of this study.

I greatly appreciate all members and graduates of the professor Ohtsuki's Laboratory for their kindness.

Akiya Akahoshi